DRAFT VERSION FEBRUARY 2, 2008
Preprint typeset using LATEX style emulateapj

arXiv:astro-ph/0502384v1 18 Feb 2005

THE MAGNETIC PROPERTIES OF AN L DWARF DERIVED FROM SIMULTANEOUS RADIO, X-RAY, AND Hα OBSERVATIONS

E. BERGER[1,2,3], R. E. RUTLEDGE[4], I. N. REID[5], L. BILDSTEN[6], J. E. GIZIS[7], J. LIEBERT[8], E. MARTÍN[9,10],
G. BASRI[11], R. JAYAWARDHANA[12], A. BRANDEKER[12], T. A. FLEMING[8], C. M. JOHNS-KRULL[13],
M. S. GIAMPAPA[14], S. L. HAWLEY[15], J. H. M. M. SCHMITT[16]

Draft version February 2, 2008

ABSTRACT

We present the first simultaneous, multi-wavelength observations of an L dwarf, the L3.5 candidate brown dwarf 2MASS J00361617+1821104, conducted with the Very Large Array, the *Chandra X-ray Observatory*, and the Kitt Peak 4-m telescope. We detect strongly variable and periodic radio emission (P = 3 hr) with a fraction of about 60% circular polarization. No X-ray emission is detected to a limit of $L_X/L_{\rm bol} \lesssim 2\times10^{-5}$, several hundred times below the saturation level observed in early M dwarfs. Similarly, we do not detect Hα emission to a limit of $L_{H\alpha}/L_{\rm bol} \lesssim 2\times10^{-7}$, the deepest for any L dwarf observed to date. The ratio of radio to X-ray luminosity is at least four orders of magnitude in excess of that observed in a wide range of active stars (including M dwarfs) providing the first direct confirmation that late-M and L dwarfs violate the radio/X-ray correlation. The radio emission is due to gyrosynchrotron radiation in a large-scale magnetic field of about 175 G, which is maintained on timescales longer than three years. The detected 3-hour period may be due to (i) the orbital motion of a companion at a separation of about five stellar radii, similar to the configuration of RS CVn systems, (ii) an equatorial rotation velocity of about 37 km s^{-1} and an anchored, long-lived magnetic field, or (iii) periodic release of magnetic stresses in the form of weak flares. In the case of orbital motion, the magnetic activity may be induced by the companion, possibly explaining the unusual pattern of activity and the long-lived signal. We conclude that fully convective stars can maintain a large-scale and stable magnetic field, but the lack of X-ray and Hα emission indicates that the atmospheric conditions are markedly different than in early-type stars and even M dwarfs. Similar observations are therefore invaluable for probing both the internal and external structure of low mass stars and sub-stellar objects, and for providing constraints on dynamo models.

Subject headings: stars: low mass,brown dwarf–stars: activity–stars: radio emission–stars: magnetic fields–radiation mechanisms: nonthermal

1. INTRODUCTION

In recent years the stellar mass function has been extended at the bottom of the main sequence and beyond with the discovery of numerous very low mass stars and brown dwarfs (spectral types late-M, L, and T; Martín *et al.* 1997; Delfosse *et al.* 1999; Martín *et al.* 1999; Reid *et al.* 1999; Luhman *et al.* 2000; Leggett *et al.* 2000; Hawley *et al.* 2002). Despite the significant observational and theoretical advances made since their discovery (e.g., Basri 2000; Chabrier & Baraffe 2000; Burrows *et al.* 2001 and references therein), many questions regarding the structure and formation of these objects remain unanswered. Not least among these is the generation, amplification and dissipation of magnetic fields and their influence on the coronae and chromospheres. In turn, these provide a window onto the physics of the internal convection, the structure of the atmosphere, and its effect on the emergent radiation. By analogy with solar-type stars and M dwarfs, we expect that the magnetic activity will be evident through coronal and chromospheric emission (X-ray, Hα, and radio).

In the M dwarfs, observations in X-rays and Hα reveal a substantial fraction of active objects, peaking at $\sim$ 70% around

[1] Observatories of the Carnegie Institution of Washington, 813 Santa Barbara Street, Pasadena, CA 91101
[2] Princeton University Observatory, Peyton Hall, Ivy Lane, Princeton, NJ 08544
[3] Hubble Fellow
[4] Department of Physics, McGill University, Rutherford Physics Building, 3600 University Street, Montreal, QC H3A 2T8, Canada
[5] Space Telescope Science Institute, 3700 San Martin Drive, Baltimore, MD 21218
[6] Kavli Institute for Theoretical Physics, University of California at Santa Barbara, Kohn Hall, Santa Barbara, CA 93106
[7] Department of Physics and Astronomy, University of Delaware, Newark, DE 19716
[8] Department of Astronomy and Steward Observatory, University of Arizona, 933 North Cherry Avenue, Tucson, AZ 85721
[9] Instituto de Astrofísica de Canarias, C/ Vía Láctea s/n, E-38200 La Laguna, Tenerife, Spain
[10] University of Central Florida, Department of Physics, PO Box 162385, Orlando, FL 32816
[11] Astronomy Department, University of California, Berkeley, CA 94720
[12] Department of Astronomy and Astrophysics, University of Toronto, 60 St. George Street, Toronto, ON M5S 3H8, Canada
[13] Department of Physics and Astronomy, Rice University, 6100 Main Street, MS-61 Houston, TX 77005
[14] National Solar Observatory, National Optical Astronomy Observatories, Tucson, AZ 85726
[15] University of Washington, Department of Astronomy, Box 351580, Seattle, WA 98195
[16] Hamburger Sternwarte, Universitat Hamburg, Gojenbergsweg 112, 21029 Hamburg, Germany

spectral type M8 (e.g., Gizis *et al.* 2000; West *et al.* 2004). Moreover, in both bands the level of activity increases with rotation velocity, up to a saturation level, at $v \sim 5$ km s^{-1}, of $L_X/L_{\rm bol} \approx 10^{-3}$ (Rosner, Golub & Vaiana 1985; Fleming *et al.* 1993; Pizzolato *et al.* 2003) and $L_{H\alpha}/L_{\rm bol} \approx 10^{-3.5}$ (Mohanty *et al.* 2002). These observations have been interpreted in the context of coronal and chromospheric heating by dissipation of magnetic fields, which in turn are powered by an internal dynamo. In stars earlier than M3 the dynamo is thought to be powered by shearing motions at the radiative-convective transition zone (the so-called $\alpha\Omega$ dynamo). The increase in activity with decreased mass and higher rotation velocity is understood as a dependence of the dynamo on the Rossby number, $Ro = P/\tau_c$, where P is the rotation period and τ_c is the convective turnover time (e.g., (Soderblom *et al.* 1993)). The saturation effect is still not fully understood.

Surprisingly, the onset of full convection and the expected breakdown of the $\alpha\Omega$ dynamo at spectral type M3 is not accompanied by obvious changes in the level of Hα and X-ray emission or the rotation-activity relation. This has been attributed to a growing contribution from an α^2 (Raedler *et al.* 1990) or a turbulent dynamo (Durney, De Young & Roxburgh 1993) in which the shearing needed to generate and amplify the fields comes from turbulent motion associated with the internal convection. However, beyond spectral type M7 there is a precipitous drop in Hα and X-ray persistent activity, and only a handful of objects exhibit flares, $\sim 7\%$ in late-M dwarfs and $\sim 1\%$ in L dwarfs (e.g., Reid *et al.* 1999; Gizis *et al.* 2000; Rutledge *et al.* 2000; Liebert *et al.* 2003; West *et al.* 2004 and see Figure 14). Furthermore, the activity-rotation relation no longer holds in late-M and L dwarfs with many rapid rotators ($v \gtrsim 20$ km s^{-1}) exhibiting no discernible activity (Basri & Marcy 1995; Mohanty & Basri 2003). The decrease in activity may be due to a quenching of the turbulent dynamo and a transition to small-scale and short-lived fields[17]. Moreover, the increasingly neutral atmospheres of late-M and L dwarfs may hamper the dissipation of the fields (Mohanty *et al.* 2002). In effect, the increased rate of collisions between charged and neutral particles may decouple the magnetic field from the atmosphere, thereby suppressing the build-up of magnetic stresses and the heating of the chromosphere and corona.

The above discussion suggests that radio emission, produced by interaction of relativistic electrons with the magnetic field, should also be suppressed in late-M and L dwarfs. Observationally, the empirical relation between the radio and X-ray luminosities of a wide range of coronally-active stars, including many M dwarfs (Guedel & Benz 1993; Benz & Guedel 1994), along with the few X-ray detections and upper limits obtained to date, suggest an expected flux level below 0.1 μJy (i.e., several hundred times lower than the detection threshold of the Very Large Array).

However, radio observations of late-M and L dwarfs present a decidedly different picture. Berger *et al.* (2001) (hereafter, B01) detected radio flares and persistent emission from the M9.5 brown dwarf LP944-20 four orders of magnitude brighter than expected based on X-ray observations (Rutledge *et al.* 2000; Martín & Bouy 2002) and the radio/X-ray correlation. A subsequent survey of twelve additional objects (Berger 2002; hereafter, B02) revealed flares and persistent emission from three objects ranging from M8.5 to L3.5. In all cases the inferred magnetic fields strengths were of the order of 100 G. In addition, of the three detected objects, the two which have been observed in X-rays again violated the radio/X-ray correlation by orders of magnitude. Recently, Putman & Burgasser (2003) detected radio emission from four out of seven M7 to L4.5 dwarfs they observed with Australia Telescope Compact Array, of which one exhibited a strong flare. Thus, the incidence rate of radio emission in late-M and L dwarfs may be as high as 40%, much larger than in Hα or X-rays.

Beyond the individual properties inferred from the unexpected radio emission, two puzzling trends have emerged. First, the fraction of persistent radio emission compared to the bolometric luminosity appears to increase with later spectral type, the exact opposite of the trend observed in Hα and X-ray activity. Second, the radio bright objects are those with high rotation velocities ($v\sin i \gtrsim 20$ km s^{-1}), while significant non-detections are associated with slow rotators ($v\sin i \lesssim 10$ km s^{-1}). This implies that the rotation-activity relation holds in the radio, despite being broken in Hα and X-rays.

The glaring disparity between the trends observed in the various activity indicators makes it clear that a complete picture of magnetic activity in late-M and L dwarfs requires simultaneous, multi-wavelength observations. These observations can furthermore constrain turbulent dynamo models, which despite significant progress are still under-developed and under-constrained. Here we present the first such observations for any L dwarf, the L3.5 object 2MASS J00361617+1821104 (hereafter, 2M0036+18). In §2 we provide the details of our radio, X-ray, and Hα observations. We summarize the results in §3 and address the radio emission mechanism and derive the magnetic field properties in §4. The violation of the radio/X-ray correlation and its implications are discussed in §5. A possible periodicity observed in the radio emission is assessed in §6 and implications for the magnetic field generation mechanism are drawn in §7. Finally, we summarize the current trends in radio, Hα and X-ray emission from M and L dwarfs in §8.

2. OBSERVATIONS

We targeted the L3.5 dwarf 2M0036+18 (Reid *et al.* 1999) due to its relative vicinity and previous observations of radio activity. The object is located at a distance of 8.8 pc (Dahn *et al.* 2002), has a bolometric luminosity, $L_{\rm bol} \approx 10^{-3.97}$ L$_\odot$ (Leggett *et al.* 2002; Vrba *et al.* 2004), a rotation velocity, $v\sin i \approx 15 \pm 5$ km s^{-1}, measured from high-resolution optical spectra (Schweitzer *et al.* 2001), an inferred temperature of about 1900 K (Vrba *et al.* 2004), an inferred radius of about 0.09 ± 0.01 R$_\odot$ (Dahn *et al.* 2002), a mass of about 0.076 M$_\odot$ inferred from the surface gravity, $\log g \approx 5.4$ (Schweitzer *et al.* 2001), and an inferred age of at least 1 Gyr (e.g., Burrows *et al.* 2001). Thus, 2M0036+18 is an object located near or below the hydrogen burning limit. 2M0036+18 has been detected in previous radio observations carried out in September and October of 2001, with a strong $\sim$ 20-min flare, variable persistent emission, and a high fraction of circular polarization (B02).

The observations presented here were carried out simultaneously in the radio, X-ray, and optical on September 28, 2002. Radio observations commenced at 01:49 UT and ended at 09:39 UT (28.2 ks), X-ray observations covered the range 01:10 to 07:17 UT (22 ks), and optical spectroscopic observations covered the range 02:47 to 07:31 UT (17 ks).

---

[17] Recent work by Dobler, Stix & Brandenburg (2004) on magnetic field generation in convective rotating stars suggests that large-scale fields can be generated and maintained on relatively long timescales. However, these authors use physical conditions relevant for an M5 dwarf (and with an unusually high surface temperature), while substantial changes in Hα and X-ray activity are manifested only for objects later than M7, and we are interested in mid-L dwarfs here.

2.1. *Radio*

Very Large Array (VLA[18]) observations were conducted simultaneously at 4.86 and 8.46 GHz in the standard continuum mode with 2×50 MHz contiguous bands at each frequency. We used fourteen antennas at 4.86 GHz and thirteen antennas at 8.46 GHz, with a staggered configuration in each of the three array arms. Eight-minute scans on 2M0036+18 were interleaved with 50 s scans on the phase calibrator J0042+233. The flux density scale was determined using the extragalactic source 3C 48 (J0137+331).

The data were reduced and analyzed using the Astronomical Image Processing System (AIPS; Fomalont 1981). The visibility data were inspected for quality, and noisy points were removed. To search for flares, we constructed light curves using the following method. We removed all the bright field sources using the AIPS/IMAGR routine to CLEAN the region around each source (with the exception of 2M0036+18), and the AIPS/UVSUB routine to subtract the resulting source models from the visibility data. We then plotted the real part of the complex visibilities at the position of 2M0036+18 as a function of time using the AIPS/UVPLT routine. The subtraction of field sources is necessary since their sidelobes and the change in the shape of the synthesized beam during the observation result in flux variations over the map, which may contaminate any real variability or generate false variability. We repeated this procedure for the background sources as a check on the intrinsic noise properties of the maps. The resulting light curves are shown in Figures 1 and 2.

We conducted follow-up observations with the VLA on 2005, Jan. 10 and 11 UT at 4.86 GHz. A total of ten hours were obtained using the same phase and flux calibrators as in the Sep. 2002 observation. We followed the same procedure outlined above to to produce light curves (Figures 8 and 9)

2.2. *X-rays*

The observations were made with the *Chandra*/ACIS-S3 (backside-illuminated chip). 2M0036+18 was offset from the on-axis focal point by 4′ to mitigate pileup in the event of a flare. Data were analyzed using CIAO v3.1. We extracted data within a 4″ circle centered on the source position, selecting counts in a low energy band (0.2-3 keV) and a total energy band (0.2-10 keV). Sources were found using `celldetect`. To estimate the background we used annuli centered at the source position, excluding other point sources detected in the observation. We adopt an energy conversion factor of 1 count = 4.5×10^{-12} erg cm^{-2} s^{-1} (0.2-8 keV), consistent with a kT=1 keV Raymond-Smith plasma.

No X-ray source is detected at the optical position of 2M0036+18. The number of counts in the low and total energy bands were 3 and 5, respectively, while we expected 2 and 4 counts from the background. There is no evidence for flaring activity, or deviation from the Poisson count rate distribution expected from a constant background. For example, the shortest time-span which includes 3 counts is 6.4 ks. For a detection of 5 counts, the 90% confidence limit (found from an average count rate of <9 counts per 21.5 ks) on the time-averaged flux is $< 1\times 10^{-15}$ erg cm^{-2} s^{-1}. We observed no more than 1 count per 1 hr time period, corresponding to a 90% confidence limit on a 1 hr average peak flux (<3 counts/hr) of $< 4\times 10^{-15}$ erg cm^{-2} s^{-1}. At the distance of 2M0036+18 the upper limit on persistent emission is $L_X \lesssim 9.3\times 10^{24}$ erg s^{-1}, or $\log(L_X/L_{\rm bol}) \lesssim -4.65$.

2.3. *Optical*

2M0036+18 was monitored spectroscopically using the Multi-Aperture Red Spectrometer (MARS) mounted on the Mayall 4-meter telescope at Kitt Peak National Observatory. A series of forty-eight 300-s exposures covering $6400-10,100$A with a resolution of 3A pix^{-1} were obtained in clear and photometric conditions with reasonable seeing ($\sim$1.2″, although the initial observations were made at airmass exceeding 2). All of the spectra were flat-fielded, extracted and wavelength calibrated using standard IRAF routines. Observations of Feige 110 were used to set the flux scale.

None of the spectra show evidence for Hα emission. The individual 300-s spectra have signal-to-noise of about 10 to 15 at these wavelengths, leading to an upper limit on the Hα equivalent width of ≈ 1.5A (or $F_{H\alpha} \lesssim 5\times 10^{-17}$ erg cm^{-2} s^{-1}). Combining all the individual spectra (Figure 3), we find no evidence for emission exceeding an equivalent width of 0.4A, or $F_{H\alpha} \lesssim 1\times 10^{-17}$ erg cm^{-2} s^{-1}. At the distance of 2M0036+18 this translates to $L_{H\alpha} \lesssim 9.3\times 10^{22}$ erg s^{-1}, or $\log(L_{H\alpha}/L_{\rm bol}) \lesssim -6.65$.

Separately, on 2004 December 5 we obtained two 10-min high-resolution spectra with the Magellan Inamori Kyocera Echelle (MIKE) Spectrograph, separated by 103 min. The purpose of this observation was to measure a possible radial velocity induced by a close-in companion (see §6). A 0.35″ slit was used with 2×2 binning, providing a spectral resolution of about 27,000 in the red or about 0.11A per pixel. The spectra were flat-fielded, rectified, wavelength calibrated and extracted using a MIKE data reduction pipeline. The rms wavelength residuals were of the order of 0.005A and the signal-to-noise in the relevant echelle orders was approximately ten and six in the first and second spectrum, respectively.

3. BASIC PROPERTIES OF THE RADIO EMISSION

While neither X-ray nor Hα emission were detected from 2M0036+18, radio emission was detected with an average flux of 259 ± 19 μJy and 134 ± 16 μJy at 4.9 and 8.5 GHz, respectively (Figure 1). The resulting spectral index ($F_\nu \propto \nu^\alpha$) is $\alpha = -1.2\pm 0.3$, typical of radio emission observed from M dwarfs (Gudel *et al.* 1993). The emission is strongly circularly polarized with an average of $f_c \approx -73\pm 8\%$ at 4.9 GHz and $f_c \approx -60\pm 15\%$ at 8.5 GHz. The negative sign indicates that the polarization direction is left-handed. We place a limit of $\lesssim 20\%$ (3σ) on the fraction of linear polarization at 4.9 GHz and $\lesssim 35\%$ at 8.5 GHz. In the follow-up observations we detected emission from 2M0036+18 at a level of 152 ± 9 μJy, with a fraction of circular polarization, $f_c \approx -46\pm 7\%$.

For comparison, two past observations of 2M0036+18 at 8.5

---

[18] The VLA is operated by the National Radio Astronomy Observatory, a facility of the National Science Foundation operated under cooperative agreement by Associated Universities, Inc.

GHz (B02) revealed a similar flux level, 135 and 330 μJy, but a lower fraction of circular polarization, –35% and –13%. One of the two observations also uncovered a 20-min flare with a peak flux of about 720 μJy and a fraction of circular polarization, $f_c \approx -62\%$. No such flares are observed here suggesting that their rate of occurrence, taking into account all three observations, is < 0.04 hr^{-1}. The flare duty cycle, defined as the flare duration relative to the total observing time, is $\lesssim 1.5\%$.

The brightness temperature of the radio emission, an important discriminant of the emission mechanism, is given by

$$T_b \approx 2\times 10^9 F_{\nu,\mathrm{mJy}} \nu_{\mathrm{GHz}}^{-2} d_{\mathrm{pc}}^2 (R/R_J)^{-2}\ \mathrm{K}, \quad (1)$$

where $R_s/R_J \approx 1$ is the radius in units of Jupiter radii. We find that $T_b \approx 2\times 10^8$ K if the emission is produced in the corona at a radius of $R \sim 3R_s \sim 3R_J$ (Linsky & Gary 1983; Burrows, Hubbard & Lunine 1989; Leto *et al.* 2000) and with a covering fraction of 100%. On the other hand, if the emission is confined to a significantly smaller region (e.g., a coronal loop with $R \lesssim 0.1R_s$) then T_b may exceed 10^{11} K. In the case of gyromagnetic radiation (see §4.1), the inverse Compton catastrophe limit, $T_b \lesssim 10^{12}$ K, defines a minimum size for the emission region of about $0.08R_s \approx 5.0\times 10^8$ cm.

4. EMISSION MECHANISM

Several radiation mechanisms can give rise to the observed radio emission (e.g., Güdel 2002): Bremsstrahlung radiation, gyromagnetic radiation, and coherent processes (plasma radiation or electron cyclotron maser). We can rule out bremsstrahlung radiation in this case since the expected spectrum is flat in the optically thin regime, whereas here $\alpha \approx -1.2$.

Coherent emission processes, which have been invoked in cases of high brightness temperature ($T_b > 10^{12}$ K) solar and stellar flares with strong circular polarization, are also unlikely in this case. This is primarily because the emission is expected to have a narrow bandwidth around the fundamental or second harmonic of the plasma frequency, $\nu_p \approx 9000 n_e^{1/2}$ Hz, or the cyclotron frequency, $\nu_c \approx 2.8\times 10^6 B$ Hz, whereas here emission is detected at both 4.9 and 8.5 GHz. In addition, the typical emission timescale of coherent radiation flares is much shorter than the 7.8-hour duration of the radio emission detected in this case.

4.1. *Gyromagnetic Radiation*

Gyromagnetic radiation can arise from a thermal or non-thermal distribution of electrons, with the latter typically assumed to follow a power law, $n(\gamma) \propto \gamma^{-p}$, above some cutoff, γ_m. The emission properties further depend on the harmonic number, s, or equivalently the typical energy of the electrons $\gamma = s^{1/3}$. Cyclotron emission is produced when $s \lesssim 10$ (non-relativistic electrons, typically thermal distribution), gyrosynchrotron when $s \approx 10-100$ (mildly relativistic electrons), and synchrotron when $s \gtrsim 100$ (relativistic electrons). The frequency at which the bulk of the radiation is emitted is given by $\nu_m \approx 2.8\times 10^6 sB$ Hz, where B is the magnetic field strength.

Cyclotron radiation is unlikely in this case since the emission is expected to be concentrated in narrow bands at the harmonic frequencies, as opposed to the detected signal at 4.9 and 8.5 GHz. Similarly, gyrosynchrotron emission from a thermal plasma is unlikely since the expected optically thin spectral index, $\alpha \approx -8$, is significantly steeper than the observed value. Finally, synchrotron emission is unlikely because the expected degree of circular polarization is strongly suppressed compared to the value of about 70% measured here. Therefore, the most likely emission mechanism in the case of 2M0036+18 is gyrosynchrotron radiation from a non-thermal distribution of electrons.

The emission properties in the gyrosynchrotron case depend both on the fundamental source parameters – magnetic field B, electron density n_e, and line-of-sight source scale L – and the angle between the line of sight and the magnetic field, θ (Dulk & Marsh 1982). Since the latter cannot be inferred from the present data we take $\theta = \pi/3$ as a representative value. The spectral index in the optically thin case, $\alpha \approx 1.2-0.9p$, indicates that $p \approx 2.7$. This value is similar to those found in several early M dwarfs (Gudel *et al.* 1993). Given the value of p, the fraction of circular polarization at 4.9 GHz is given by $f_c \approx 0.025B^{0.53} \approx 0.6$, from which we infer $B \approx 400$ G. For the full range of possible θ values the magnetic field strength ranges from about 80 to 1.9×10^3 G. These values indicate that the harmonic number is $s < 22$, with the gyrosynchrotron limit, $s > 10$, corresponding to $B < 175$ G, or $\theta < \pi/4$. Below we use the latter value for the magnetic field strength.

The frequency at which the gyrosynchrotron spectrum peaks is given by $\nu_m \approx 6.1\times 10^5 (n_e L)^{0.24} < 4.86\times 10^9$ Hz, while the flux in the optically thin regime is $F_\nu \approx 1.1\times 10^{-34} n_e L R^2 \approx 205$ μJy, using the average flux at 4.9 GHz. Solving for the unknown column density and radius of the emission region we find $n_e L < 1.8\times 10^{16}$ cm^{-2} and $R \approx 1\times 10^{10}$ cm, or about $1.4R_s$. The resulting brightness temperature is $T_b \approx 7\times 10^8$, consistent with the interpretation of the radio emission as gyrosynchrotron radiation. Assuming that $L = R$, the electron density is $n_e \approx 1.6\times 10^6$ cm^{-3}.

Several conclusions can be drawn from this discussion. First, the magnetic field strength is larger than the average solar field or the magnetic field of Jupiter, but is somewhat lower than the ~ 1 kG fields inferred in some active early M dwarfs (Smith *et al.* 1975; Saar & Linsky 1985; Haisch, Strong & Rodono 1991; Johns-Krull & Valenti 1996; Stepanov *et al.* 2001). We note however, that the surface magnetic field of 2M0036+18 may be an order of magnitude larger than that inferred for the emission region if $L \approx R \approx 1.4R_s$, placing it in the same range of early M dwarfs. Second, the radio emission, and in particular the high fraction of circular polarization, requires a large-scale, long-lived ordered magnetic field with a large covering fraction. This is again similar to the conditions inferred for early M dwarfs (Saar & Linsky 1985; Johns-Krull & Valenti 1996). Finally, the density of emitting electrons is similar to that inferred in the emission zones (coronae) of early M dwarfs (Stepanov *et al.* 2001; Osten *et al.* 2004). Thus, the physical conditions in the L3.5 2M0036+18 resemble those found in active early M dwarf, but the Hα and X-ray emission are strongly suppressed.

We finally note that the plasma-beta, $\beta = 2\mu_0 P/B^2$, of the corona, using $n \sim 1.6\times 10^6$ cm^{-3}, a typical temperature $T \sim 2\times 10^6$ K (Giampapa *et al.* 1996), and $B \sim 175$ G, is $\beta \sim 3\times 10^{-8}$. The typical photospheric pressure of an L dwarf is $P \sim 3\times 10^5$ dyne cm^{-2} (Burrows *et al.* 2001), resulting in $\beta \sim 2$. These conditions are again similar to those found in M dwarfs (Giampapa *et al.* 1996) and the Sun. Thus, even small perturbations in the coronal field of 2M0036+18 are capable of supporting the pressure gradients produced by the radio-emitting material.

5. VIOLATION OF THE RADIO/X-RAY CORRELATION

The simultaneous radio and X-ray observations allow us for the first time to directly investigate the radio/X-ray correlation in an L dwarf. Similar observations of coronally active stars (including the Sun) reveal a tight correlation between L_R and L_X (Figure 4; Guedel & Benz 1993; Benz & Guedel 1994). This correlation holds for both flaring and persistent emission, and for single stars and binary systems. For M dwarfs the correlation holds to spectral type M7 (Gudel *et al.* 1993). The persistent emission follows $L_R \approx 3\times10^{-16} L_X$ Hz^{-1} (Guedel & Benz 1993), and extends over six orders of magnitude in L_R. The relation for radio and X-ray flares is non-linear, $L_R \propto 1.3\times10^{-26} L_X^{0.73}$ Hz^{-1} (Benz & Guedel 1994), and holds over eight orders of magnitude in L_R.

For 2M0036+18 we find $L_R \approx 2.5\times10^{13}$ erg s^{-1} Hz^{-1} and $L_X < 9.7\times10^{24}$ erg s^{-1}. Thus, $L_R/L_X \gtrsim 2.6\times10^{-12}$ Hz^{-1} is at least 8600 times higher than predicted by the radio/X-ray correlation (Figure 4). A similar result, from non-simultaneous data, was obtained for the M9.5 brown dwarf LP944-20 (B01) with a ratio that exceeded the expected value by a factor of 10^4 (flares) and >8500 (persistent emission). Similarly, for the M9.5 dwarf BRI 0021-0214 the radio luminosity exceeded the X-ray upper limit by at least a factor of 10^3 (B02). Thus, the radio and X-ray luminosities appear to de-correlate over a narrow range in spectral type (between about M7 and M9) and remain uncorrelated at least to mid-L (Figure 4). Incidentally, this is the same range over which both the fraction of Hα and X-ray active sources and the strength of the activity drop precipitously.

The violation of the radio/X-ray correlation is surprising given that the magnetic and emission region properties derived for 2M0036+18 are not dissimilar from those found on early M dwarfs (§4.1). This suggests that either the origin of the magnetic field is different than in M dwarfs or the atmospheric conditions are not conducive for the support of a chromosphere and/or a corona.

The radio/X-ray correlation has been interpreted in the context of magnetic reconnection. In this scenario, the flares are produced when coronal magnetic loops reconnect, release energy, and create a current sheet along which ambient electrons are accelerated. The accelerated electrons drive an outflow of hot plasma into the corona as they interact with and heat the underlying chromospheric material. The interaction of the outflowing plasma with the electrons produces X-ray emission via the bremsstrahlung process (Neupert 1968; Hawley *et al.* 1995; Guedel *et al.* 1996). This so-called Neupert effect points to a causal connection between particle acceleration, which is the source of radio emission, and plasma heating, which results in X-ray emission. Thus, the X-ray thermal energy should simply be related by a constant of proportionality to the integrated radio flux.

Guedel & Benz (1993) discuss this correlation in terms of the relation $L_R/L_X \approx 10^{-22} B^{2.5}(a/b)\tau_0(1+\alpha)$ Hz^{-1}, where a is the fractional efficiency of accelerating electrons, b is the fraction of coronal energy radiated in X-rays, τ_0 is the average lifetime of the low-energy electrons, and α is the power law relating the electron lifetime to its energy. The observed tight correlation suggests that the combination $B^{2.5}(a/b)\tau_0$ is nearly unchanged for a wide range of stars. Since in the case of 2M0036+18 and the other radio active late-M and L dwarfs L_R/L_X is higher by several orders of magnitude while the inferred value of B is not unusual compared to M dwarfs, this indicates that either the fraction of energy emitted in X-rays, b, is suppressed by a factor of $\sim 10^4$, or the typical lifetime of the electrons, τ_0, is longer by a similar factor. In particular, for a/b of order unity and $B \approx 175$ G, we find a mean electron lifetime $\tau \sim 1$ d. In this case, the X-ray emission is suppressed because the electrons do not lose their energy to coronal heating on a sufficiently rapid timescale.

On the other hand, the violation of the radio/X-ray correlation may be due to an inefficient production of X-rays, i.e., a low value of b. In the case of L dwarfs this may be explained by the increasingly neutral atmospheres and the reduction in the density of ions available for X-ray emission (Mohanty *et al.* 2002). However, it is not clear if this can account for the late-M dwarfs LP944-20 and BRI 0021-0214, or for the sudden transition between spectral types M7 and M9. More likely, the reduction in X-ray luminosity, or the over-production of radio emission, may be related to the magnetic structure across the atmosphere, chromosphere and corona or efficient trapping of the electrons (i.e., long lifetime). We note that recent radio and X-ray observations of the dM4.5e star EV Lac also reveal a breakdown of the Neupert effect, which Osten *et al.* (2004) interpret in the same context discussed here, namely efficient trapping or a low value of b.

6. VARIABILITY AND PERIODICITY

To this point we have discussed the properties of the integrated radio emission during the entire 7.8 hour simultaneous observation and the follow-up observations. However, from Figures 1, 2, 8, and 9 it is clear that both the total intensity and circularly polarized emission at 4.9 GHz are strongly variable. For the total intensity light curve the reduced χ^2 assuming a constant flux is $\approx 2.5-7.5$ for a time resolution ranging from 5 min to 1 hour; for the circular polarization light curve $\chi^2_r \approx 1.8-2.8$ over the same range of time resolutions. It is not clear if the variability of the weaker emission at 8.5 GHz is significant, with $\chi^2_r \approx 1-1.7$ depending on the time resolution.

We are confident that this variability is not an observational artifact for two reasons. First, the light curves of two field sources, constructed in the same manner as that of 2M0036+18 (see §2.1), do not exhibit significant variability, with $\chi^2_r \approx 1.2$ and ≈ 1.8 for a time resolution of 10 min. In fact, the reduced χ^2 values for the field sources are over-estimated compared to those for 2M0036+18 since, unlike 2M0036+18, these sources are spatially extended and positioned away from the phase center. As a result, changes in the synthesized beam during the observation affect their light curves more significantly than that of 2M0036+18. Second, the variability of 2M0036+18 is significant in circular polarization where no field sources, which can introduce false variability, produce detectable emission. It is important to note that in the two past observations of 2M0036+18, lasting 150 and 180 minutes, the persistent emission was also variable (B02).

In addition to the variability, it appears from Figures 2, 8, and 9 that the radio emission at 4.9 GHz is periodic. The autocorrelation function (ACF) of both the total intensity and circular polarization at a wide range of time resolutions shows a clear peak at 3 hours (Figures 5 and 10). The ACFs of the two field sources described above are flat, as expected for non-periodic sources.

We assess the statistical significance of the 3-hour periodicity using two other methods which provide a measure of the power spectrum and are therefore more easily calibrated: The Lomb-Scargle (LS) periodogram (e.g., Press *et al.* 1992), and a one-dimensional CLEAN algorithm (Roberts, Lehar & Dreher 1987). The latter method has the added advantage that artifacts and spectral leakage which arise from the sampling function and the finite length of the observation are removed.

We assess the significance of the results using the Monte Carlo method. Specifically, we construct both randomized versions of the 4.9 GHz light curves, and simulated light curves with a (χ^2) variability similar to that of 2M0036+18. Depending on the time resolution we use $50,000$ to $100,000$ light curves in each set and perform the same procedures as on the real data. The significance of peaks in the LS and CLEAN power spectra of the real light curve are determined as the fraction of simulated light curves which produce stronger peaks. We find that both the randomized and simulated sets provide a similar measure of the significance, as do the LS and CLEAN procedures. A representative LS periodogram is shown in Figure 6.

The significance of peaks in the LS and CLEAN power spectra does depend on the choice of time resolution. This is expected since as the period is sampled more coarsely the strength of the signal is expected to decrease. We use time resolutions ranging[19] from 2 to 30 min (Figure 7), and find that the strongest peak always occurs at a frequency of 0.33 hr^{-1}, or a period of 3 hours. For the simulated light curves the peaks that exceed the value for 2M0036+18 occur over the entire frequency range. We also find that the significance of the periodicity in the circular polarization light curve is consistently higher than for the total intensity light curve. This is expected because the contamination from field sources is non-existent in circular polarization. For the range of time resolutions investigated we find that the significance of the 3-hour period peaks at $\approx 99.999\%$ for $\delta t = 2$ min. This result is confirmed by the follow-up observations, and a phased light curve of the data from 2005, Jan. 10 and 11 UT, folded with a period of 184 min is shown in Figure 11.

Thus, the radio emission from 2M0036+18 is periodic with $P = 3$ hours. This period is maintained on timescales of at least two years. If related to the rotation of 2M0036+18 then using $R_s \approx 6.3 \times 10^9$ cm, the inferred period indicates a surface equatorial rotation velocity $v \approx 37$ km s^{-1}. This value is nearly 2.5 times higher as that inferred from high-resolution optical spectra, $v\sin i \approx 15 \pm 5$ km s^{-1} (Schweitzer *et al.* 2001), suggesting an inclination angle, $i \approx 24 \pm 8^\circ$. Alternatively, if the period is related to the orbital motion of a companion which induces magnetic activity (see below) then the semi-major axis is about 3.1×10^{10} cm or about five times the stellar radius; this is similar to the case of the highly active RS CVn systems (e.g., Mutel & Lestrade 1985). Finally, the periodic rise in flux may be a series of weak flares, rather than variable persistent emission, in which case the flare generation process is periodic.

7. THE ORIGIN OF THE MAGNETIC ACTIVITY IN 2M0036+18

The results presented in the previous sections directly confirm for the first time that the relative activity patterns in late-M and L dwarfs differ from those in early-type stars and early M dwarfs. It is therefore crucial to address the origin of the magnetic fields in the well-studied 2M0036+18 as an example of a larger trend that is emerging in sub-stellar objects. While some dynamo models for convective stars predict a reduced strength, physical scale, and lifetime of the magnetic field (e.g., Durney, De Young & Roxburgh 1993), the extent of this reduction is still not known. Clearly, the stability of the magnetic field of 2M0036+18 over a period of three years indicates a long-lived process. Similarly, the physical scale of the field, $R \sim R_s$, is significantly larger than the physical scale of the convection. Finally, the inferred field strength and electron densities are similar to those inferred in early M dwarfs. It is therefore possible that the current turbulent dynamo theories are missing some key ingredients, or that the magnetic fields are generated and amplified in another process, possibly by interaction with a close-in companion.

7.1. *The Influence of a Close-in Companion*

The enhancement of magnetic fields by a close companion may play a role in the RS CVn class of active short-period binaries, and a comparison is therefore particularly illustrative. These systems are known to produce radio gyrosynchrotron emission from magnetic fields of about 200 G, with a typical luminosity of $L_{\nu,R} \approx 2 \times 10^{16}$ erg s^{-1} Hz^{-1}, a factor of 10^3 higher than that from 2M0036+18. Using the scaling for gyrosynchrotron emission, $L_{\nu,R} \propto B^{-3/4} R_s^2$, and taking into account the similar magnetic field strengths and covering fractions, as well as the ratio of radii (0.09 $\mathrm{R}_\odot$ vs. ~ 2 $\mathrm{R}_\odot$), we find $L_{\nu,\mathrm{2M}}/L_{\nu,\mathrm{RS\,CVn}} \approx 2 \times 10^{-3}$, in close agreement to the measured ratio. In addition, the ratio $L_{\nu,R}/L_{\rm bol}$ for RS CVn systems is known to be correlated with the orbital period of the system, such that tighter binaries are more radio active (Mutel & Lestrade 1985; Drake, Simon & Linsky 1989). Extrapolating this relation to the value $L_{\nu,R}/L_{\rm bol} \approx 6 \times 10^{-17}$ Hz^{-1} for 2M0036+18 we predict an orbital period of about 1 hour. This is not so dissimilar from the period of 3 hours inferred here. Thus, it is possible that 2M0036+18 represents a low-mass scaled version of the RS CVn binaries and that the same type of interaction that enhances the magnetic fields in RS CVn systems may take place here.

Another illustrative example is the recent detection of enhanced chromospheric Ca II H & K emission from the star HD 179949 orbited by a 0.84 M_J planet with an orbital period of about 3.09 days, or a semi-major axis of 6.7×10^{11} cm (Shkolnik, Walker & Bohlender 2003). The emission appears to be periodic and in phase with the orbit of the planet. The conclusion drawn by Shkolnik, Walker & Bohlender (2003) is that the planet induces magnetic activity on the stellar surface which gives rise to chromospheric emission.

These diverse examples illustrate that interaction with a companion may enhance activity. In this context both tidal and magnetic effects can play a role (Cuntz, Saar & Musielak 2000). In the case of tidal interaction, if the orbital and rotation velocities are not the same, the generation of time-varying tidal bulges may give rise to increased turbulent motions or an enhanced α-effect. The synchronization timescale (e.g., Goldreich & Soter 1966) for a companion orbiting 2M0036+18 is long, $t_{\rm sync} \approx Q_s \omega (R_s^3/GM_s)(M_s/M_p)^2 (a/R_s)^6 \approx 1.6 M_{s,J}$ Gyr; a subscript p designates the primary, a subscript s designates the secondary, ω is the angular velocity, and a is the orbital separation. Thus, it is likely that the putative companion is not tidally locked and tidal interaction may be an effective mechanism.

---

[19] We do not investigate time resolutions smaller than 2 min since the computation time becomes prohibitively long.

The strength of the tidal effect depends sensitively on both the binary separation and the mass ratio, $\Delta g_p/g_p \propto (M_s/M_p)[R_p/(a-R_p)]^3$. This suggests that the tidal effect may be particularly effective for late-M and L dwarfs where the primary mass is low and the mass ratio may thus be of order unity. For example, for the HD 179949 system the distortion is $\Delta g_p/g_p \approx 1.3\times10^{-6}$, while in the case of 2M0036+18 assuming a Jupiter-mass companion and using $a \approx 5R_p$ we find $\Delta g_p/g_p \approx 3\times10^{-4}$.

Direct magnetic interaction is also possible, with the magnetic energy of the system proportional to the product of the primary and secondary field strengths (Cuntz, Saar & Musielak 2000). In this case the energy is $E_B \propto B_p B_s/d^2_{m,p} d^2_{m,s}$, where $d_{m,s}$ is the magnetospheric radius of the secondary and $d_{m,p} \equiv a - d_{m,s}$ is the distance from the primary to that radius. The energy flux is related to E_B via $F \propto \epsilon E_B v_c$, where ϵ is an efficiency factor and v_c is the combined velocity of the stellar magnetic motions (or turbulence) and the relative velocity of the orbit (at the stellar surface) compared to the rotation of the star. Thus, as in the case of tidal interaction, the possible larger mass ratio and small separation in the case of 2M0036+18 suggests that this mechanism may be more efficient than in extra-solar planets orbiting solar-type stars.

A final possibility is that a brown dwarf companion to 2M0036+18 may undergo sustained Roche lobe overflow which may result in enhanced activity (Burgasser *et al.* 2000, 2002). This scenario has been proposed for Hα active dwarfs, although no direct evidence was found to support this hypothesis. Here we may for the first time have the required evidence. For sustained overflow to occur, the logarithmic change in radius of the secondary, $d\ln R_L/d\ln \mathrm{M_s} < -1/3$, requires a mass ratio $q \equiv M_s/M_p < 0.63$. The period is given by $P^2 = 4\pi^2 a^3/GM_p(1+q)$ while the radius of the secondary is equal to the Roche lobe radius, $R_s = R_L = 0.49aq^{2/3}/[0.6q^{2/3} + \ln(1+q^{1/3})]$. The radius of the secondary is also given by $R_s = (4/3)\pi(qM_p)^{-1/3}/[1+1.8(qM_p)^{-1/2}]^{4/3}$ (Zapolsky & Salpeter 1969; Stevenson 1991), where the constant of $4/3$ is appropriate for an age of $1-5$ Gyr (Burgasser *et al.* 2002). Using $P = 3$ hr and $M_p = 0.076$ $\mathrm{M}_\odot$ we find $q \approx 0.14$, consistent with sustained mass transfer, a secondary mass $M_s \approx 13$ M_J, a secondary radius $R_s \approx 1.1$ R_J, and an orbital separation $a \approx 5.2R_p$.

Is there a way to directly test the hypothesis of a close-in companion? As in the case of planetary companions around solar-type stars, radial velocity, astrometric shift, and photometric techniques may provide an answer. The expected radial velocity amplitude (assuming zero eccentricity) in the case of 2M0036+18 is $A \approx 2.3\times10^3(P/3\,\mathrm{hr})^{-1/3}(M_s \sin i_o/M_J)(M_p/0.076M_\odot)^{2/3}$ m s^{-1} for a Jupiter-mass companion. Using a cross-correlation of the four strongest and narrowest absorption features of 2M0036+18 (Figure 12) we obtain a limit of $A < 4$ km s^{-1} from the pair of MIKE spectra separated by about half a period (Figure 13). This indicates that $M_s \sin i_o < 1.7$ M_J if the limit is on the maximum amplitude. Naturally, if the two epochs were obtained when the putative companion was located $\sim 90°$ away from the line of sight to 2M0036+18, the lack of a radial velocity signature does not provide a useful limit.

For an orbital inclination $\cos i_o < (R_p+R_s)/a$, or $i_o \gtrsim 68°$, we expect to observe an eclipse as the companion occults 2M0036+18 ($i_o = 0°$ corresponds to a face-on orbit). For $i_o \gtrsim 73°$ more than half the surface of 2M0036+18 would be occulted resulting in large photometric variability. If all inclinations are equally likely, the probability of eclipse is about 24%. Gelino *et al.* (2002) find no significant variability for 2M0036+18 in their I-band study of photometric variability in L dwarfs. Observations were obtained with a time separation as short as $1-2$ hours, while the maximum time baseline investigated was 53 days. The lack of variability indicates that $i_o < 68°$ *if* 2M0036+18 is in fact orbited by a close companion.

Finally, a companion will induce an astrometric shift given by $\theta \approx 0.1 M_s M_p^{2/3}(P/3\,hr)^{2/3}$ mas for a $2:1$ mass ratio. This is just within the reach of current Very Long Baseline Interferometry (VLBI) observations, but lower mass ratios will result in an undetectable shift. In principle, an astrometric shift down to a mass ratio of $50:1$, or $M_s \approx 1.7$ M_J, may be detected with the 4 μas precision of the Space Interferometry Mission (SIM).

7.2. *Magnetic Structure and Rotation*

The 3-hour period may alternatively be due to the rotation of 2M0036+18. Using the inferred radius of 0.09 $\mathrm{R}_\odot$, the equatorial velocity is 37 km s^{-1}, leading to an inclination angle of $24\pm8°$, or nearly pole-on. The azimuthal orientation, ϕ, of the axis of rotation relative to the line of sight is not known. However, given the low inclination and the large covering fraction, the radio-emitting region has to be located at a low latitude for most ϕ values. This is because a location near the pole would make the bulk of the region visible throughout the rotation period, resulting in a nearly constant flux level. As can be seen from Figure 2 the flux drops to nearly zero between the peaks indicating the emission region is fully occulted for about half the rotation period. We note also that the low inclination may explain the constant sign of the circular polarization since for most values of ϕ only one of the hemispheres is visible.

If the 3-hour period is related to the rotation of 2M0036+18 then we can estimate the Rossby number, $Ro = P/\tau_c$, which is relevant for dynamo models. The convective turnover time for 2M0036+18 is $\tau_c = (MR^2/L)^{1/3} \approx 0.8$ yr indicating that $Ro \approx 4.4\times10^{-4}$. At such low values early M dwarfs exhibit saturated X-ray emission, $L_X/L_{\mathrm{bol}} \sim 10^{-3}$ (Pizzolato *et al.* 2003). Clearly, the conditions in L dwarfs are sufficiently different that a low Rossby number does not result in X-ray emission. We also note that the large value of τ_c may explain the stability of the radio emission (flux and circular polarization) over a period of about three years.

7.3. *Periodic Flaring*

Finally, it is possible that the variable persistent emission is in fact a series of periodic flares with a rate of occurrence of about 0.33 hr^{-1}. The frequency of strong flares, similar to the one detected by B01 with a flux of about 720 μJy, is $\lesssim 0.04$ hr^{-1}. This pattern is similar to the case of the M9 dwarf LHS 2065 for which strong Hα flares have an occurrence rate of $\lesssim 0.03$ hr^{-1} while weak flares occur at a rate as high as about 0.5 hr^{-1} (Martín & Ardila 2001). If this is the case here, then the timescale to build up magnetic stresses is about 3 hours, while the lifetime of the electrons, corresponding to the width of the flares, is about 1 hour.

In this scenario it is possible that the periodic weak flares are inefficient at heating the corona and chromosphere, thus explaining the lack of accompanying X-ray and Hα emission. The more rare strong flares, on the other hand, with an impulsive energy release a few times larger may be accompanied by efficient heating. However, we note that the time-integrated energy release in the putative flares observed here, $E \sim \nu L_\nu t \sim 4 \times 10^{26}$ erg, is not so different from the integrated energy release inferred for the stronger flare (B02).

8. EMERGING ACTIVITY PATTERNS OF LATE-M AND L DWARFS

The growing sample of late-M and L dwarfs observed in the radio and X-rays allows to investigate the patterns of activity as a function of relevant physical parameters. Hα observations of late-M and L dwarfs indicate a significant drop in the level of emission compared to the bolometric luminosity (Figure 14). Objects earlier than about M6 tend to have a ratio $L_{H\alpha}/L_{\rm bol}$ in the range of 10^{-4} to 10^{-3}. However, by spectral type L0 this ratio is typically lower than 10^{-5}. The few late-M and L dwarfs which exhibit flares ($\sim 1\%$; Liebert *et al.* 2003) appear to have levels of emission similar to those of early M dwarfs, with only a single source exceeding that level to date. Thus, Hα emission drops significantly with a decreased surface temperature (later spectral type), and flares exceeding the saturation value are extremely rare.

Similarly, the ratio $L_X/L_{\rm bol}$ drops from a saturation value of about $10^{-2.5}$ in mid-M dwarfs to less than 10^{-4} for the few late-M dwarfs observed to date (e.g., Fleming *et al.* 1993; Rutledge *et al.* 2000; Martín & Bouy 2002). With the exception of a recently-discovered M9 dwarf for which a ratio of about 0.1 was measured during a flare (Hambaryan *et al.* 2004), the flares observed in other late-M dwarfs do not exceed the saturation level observed in the mid-M dwarfs (Stelzer 2004). Thus, in both Hα and X-rays the saturation effect appears to be real, with flares replacing persistent emission in late-M and L dwarfs. 2M0036+18 appears to follow the general trend with upper limits on the X-ray and Hα emission that are about three orders of magnitude below the respective saturation values.

On the other hand, the radio activity in late-M and L dwarfs, and in particular 2M0036+18, exhibits a completely different trend. The observed ratio $L_R/L_{\rm bol}$ is about 10^{-8} for persistent emission from early and mid-M dwarfs. However, the level of radio emission from late-M and L dwarfs exceeds this value by about an order of magnitude, while flares are brighter by at least two orders of magnitude. 2M0036+18 in particular has a ratio $L_R/L_{\rm bol}$ of about $10^{-6.2}$. Thus, while a significantly smaller number of objects have been observed in the radio compared to Hα, *every* single detection is brighter than the value observed in mid-M dwarfs. Moreover, the fraction of detected objects is much higher, $\sim 40\%$. This suggests that a saturation effect does not exists in the radio band. Moreover, the radio luminosity does not seem to decrease with surface temperature.

Another important trend, proposed by B02, is that rapid rotators exhibit stronger radio activity. This is shown in Figure 15. In Hα there is a clear rotation-activity relation in dwarfs earlier than M7, but this relation clearly breaks down in late-M and L dwarfs. A similar relation exists in X-rays, but it again breaks down in late-M and L dwarfs. In the radio band, on the other hand, the rotation-activity relation appears to extend to late-M and L dwarfs. The only objects for which the ratio of radio to bolometric luminosity is lower than the detected objects are those with $v\sin i \lesssim 10$ km s^{-1}.

Thus, it appears that the efficiency of magnetic field generation and dissipation in fact does not decrease in late-M and L dwarfs, but the efficiency of chromospheric and coronal emission does. Similarly, the rotation activity relation appears to still hold, but the activity is manifested in radio emission instead of Hα or X-rays. The detection of rare Hα and X-ray flares does suggest that chromospheric and coronal heating may still occur, but this may require large reconnection events, possibly accompanied by large radio flares.

9. CONCLUSIONS

The simultaneous, multi-wavelength observations presented in this paper provide unparalleled insight into the magnetic field properties of an L dwarf. Most importantly, these observations directly confirm that radio activity is more prevalent in late-M and L dwarfs compared to Hα and X-ray activity. The detection rate in the radio may be as high as 40%, while in Hα it is at most a few percent. Only a few objects later than M7 have been observed in the X-rays, but persistent emission is clearly rare. A detailed analysis of the radio emission along with the lack of detectable X-ray and Hα emission give rise to the following inferences:

1. The radio emission from 2M0036+18, as compared to the bolometric luminosity, is the strongest observed in any dwarf star to date. Moreover, the emission from 2M0036+18 violates the radio/X-ray correlation by at least four orders of magnitude suggesting a drastic change in the coronal and chromospheric conditions compared to those observed in active stars down to spectral class M7. This is the first direct confirmation of this violation which has been observed in two additional late-M dwarfs (B01; B02).

2. The radio emission is due to gyrosynchrotron radiation in a magnetic field of about 175 G. The size of the emission region is about 10^{10} cm ($\sim 1.4 R_s$), indicating a large covering fraction at the surface. These characteristics are similar to those inferred in early M dwarfs.

3. The constant fraction and sense of the circular polarization in observations conducted over a period of more than three years, implies that an ordered magnetic field is maintained stably on long timescales, despite the occasional production of strong flares (B02); the incidence rate for the latter is < 0.04 hr^{-1}.

4. The radio emission is periodic ($\gtrsim 99.999\%$ confidence level) with a period of 3 hours. If related to the rotation period this indicates a rotation velocity of about 37 km s^{-1}, while if related to an orbital period it indicates a semi-major axis of about five times the stellar radius. Alternatively, the period may be due to periodic release of the magnetic energy in the form of weak radio flares.

Clearly, the radio emission from 2M0036+18 requires a large-scale, long-lived, and relatively strong magnetic field. The lack of accompanying Hα and X-ray emission suggests that the general decline in these activity indicators in late-M and L dwarfs is not a reliable tracer of decreased magnetic activity. In particular, if the magnetic field is essentially decoupled from gas in the cool atmospheres of late-M and L dwarfs so that magnetic stresses are suppressed, this may quench the chromospheric and coronal emission. However, at larger distances the rate of collisions between charged and neutral particles may drop and the field could then couple effectively to the gas (Mohanty *et al.* 2002). This is the region where radio emission is expected to be generated most effectively, explaining the strong radio signal compared to the reduced Hα and X-ray emission. However, even this scenario cannot easily account for the severe violation of the radio/X-ray correlation, or for the detection of Hα and X-ray flares from some L and T dwarfs.

While the origin of the observed periodicity remains unknown, all three scenarios provide interesting constraints for turbulent dynamo models. In the case of periodicity due to a close-in companion, it is possible that the magnetic field of 2M0036+18 is amplified by interaction with the companion. This may alleviate the need to generate strong, long-lived fields from convection alone. If the incidence of activity in the radio band is truly 40%, this may also require an unusually high fraction of companions, especially in comparison to current estimates of the binary fraction in late-M and early L dwarfs of $\sim 15\%$ (Close *et al.* 2003; Gizis *et al.* 2003). However, this fraction is estimated primarily from direct detection with AO systems and the *Hubble Space Telescope* which are only sensitive to companions at separations of $\gtrsim 1$ AU, several hundred times larger than the possible orbit in the case of 2M0036+18. Direct evidence for close-in companions is required before strong claims can be made, but radio active late-M and L dwarfs may provide a signpost for binary systems.

On the other hand, in the case of periodicity due to rotation, it is clear that any dynamo model has to explain the presence of magnetic structures similar to those of M dwarfs without the benefit of a radiative-convective transition zone and without hydrogen burning as a source of heat. Obviously, if the observed radio emission is in fact due to a series of episodic flares, this places stringent constraints on the timescale of magnetic field amplification and dissipation (~ 1 hour) over a large fraction of the stellar surface.

The multi-wavelength approach taken in this paper is clearly the first step in addressing the details of magnetic field generation at the bottom of the main sequence and beyond. Continued studies, particularly in the radio and X-ray poorly-sampled range M9 to L5 (Figure 14), are essential for understanding individual objects, as well as the effects of various physical properties (e.g., binarity, rotation, temperature, age). These observations will for the first time provide robust constraints for dynamo models and for the structure of late-M and L dwarfs all the way from the interior to the corona.

We thank first and foremost Barry Clark (NRAO), Scott Wolk (CXC, HEAD), and Meghan McGarry (CXC, HEAD) for their efforts in scheduling the simultaneous VLA and Chandra observations. Support for this work was provided by NASA through Chandra Award Number GO2-3012B issued by the Chandra X-Ray Observatory center, which is operated by SAO for and on behalf of NASA under contract NAS8-39073. Further support was provided by National Science Foundation grant NSF PHY 99-07949. EB is supported by NASA through Hubble Fellowship grant HST-01171.01 awarded by the Space Telescope Science Institute, which is operated by AURA, Inc., for NASA under constract NAS 5-26555.

APPENDIX

X-RAY OBSERVATIONS OF THE L5 DWARF 2MASS J15074769-1627386

In addition to the X-ray observations of 2M0036+18 outlined in this paper, we also observed the L5 dwarf 2MASS J15074769-1627386 (hereafter, 2M1507-16; Reid *et al.* 2000; Kirkpatrick *et al.* 2000) as part of our *Chandra* AO3 program. This object is located at a distance of 7.4 pc (Reid *et al.* 2000, 2001; Dahn *et al.* 2002), has a surface temperature of about 1630 K, a bolometric luminosity of $10^{-4.27}$ $L_\odot$, an inferred radius of 0.09 $R_\odot$ (Vrba *et al.* 2004), and a rotation velocity $v\sin i \approx 27$ km s^{-1} (Bailer-Jones 2004). The upper limit on Hα emission is $L_{H\alpha}/L_{\rm bol} < 10^{-5.76}$ (Reid *et al.* 2000) and no Li is detected to a limit of 0.1A. Finally, B02 find an upper limit on the radio luminosity at 8.5 GHz of 3.8×10^{12} erg s^{-1} Hz^{-1} from a 2.2-hr observation, corresponding to $L_R/L_{\rm bol} \lesssim 10^{-6.8}$.

The details of the X-ray observation and data analysis are given in §2.2. No X-ray source is detected at the position of 2M1507-16. The number of counts in the low and total energy bands were 2 and 4 respectively, while we expect 2 and 5 counts from background alone. We find no evidence for variability: In the total energy band, the shortest time-span which includes 3 counts is 2330 s, which we find from a Monte Carlo simulation, will occur in 22% of 27.7 ks light curves containing four counts. The 90% confidence limit on the time-averaged flux (<7 counts per 27.7 ks) is $< 1 \times 10^{-15}$ erg cm^{-2} s^{-1}. Taking the 3 counts within 2330 s, we place a 90% confidence upper limit on a 1-hr peak flaring flux of $< 1 \times 10^{-14}$ erg cm^{-2} s^{-1}. At the distance of 2M1507-16, the upper limit on persistent emission is $L_X \lesssim 6.6 \times 10^{24}$ erg s^{-1}, or $\log(L_X/L_{\rm bol}) \lesssim -4.5$.

The upper limits on X-ray, radio, and Hα activity for 2M1507-16 are shown in Figures 14 and 15. Clearly this object follows the general trend of decreased Hα and X-ray activity in L dwarfs. The radio activity is at least a factor of four lower than that of 2M0036+18, but the upper limit is several times brighter than other late-M and L dwarfs with a similar rotation velocity.

References

Bailer-Jones, C. A. L. 2004, A&A, 419, 703.

Basri, G. 2000, ARA&A, 38, 485.

Basri, G. and Marcy, G. W. 1995, AJ, 109, 762.

Benz, A. O. and Guedel, M. 1994, *A&A*, 285, 621.

Berger, E. 2002, ApJ, 572, 503.

Berger, E. *et al.* 2001, Nature, 410, 338.

Burgasser, A. J., Kirkpatrick, J. D., Reid, I. N., Liebert, J., Gizis, J. E., and Brown, M. E. 2000, AJ, 120, 473.

Burgasser, A. J., Liebert, J., Kirkpatrick, J. D., and Gizis, J. E. 2002, AJ, 123, 2744.

Burrows, A., Hubbard, W. B., and Lunine, J. I. 1989, ApJ, 345, 939.

Burrows, A., Hubbard, W. B., Lunine, J. I., and Liebert, J. 2001, Reviews of Modern Physics, 73, 719.

Chabrier, G. and Baraffe, I. 2000, ARA&A, 38, 337.

Close, L. M., Siegler, N., Freed, M., and Biller, B. 2003, ApJ, 587, 407.

Cuntz, M., Saar, S. H., and Musielak, Z. E. 2000, ApJ, 533, L151.

Dahn, C. C. *et al.* 2002, AJ, 124, 1170.

Delfosse, X., Tinney, C. G., Forveille, T., Epchtein, N., Borsenberger, J., Fouqué, P., Kimeswenger, S., and Tiphène, D. 1999, A&AS, 135, 41.

Dobler, W., Stix, M., and Brandenburg, A. 2004, astro-ph/0410645.

Drake, S. A., Simon, T., and Linsky, J. L. 1989, ApJS, 71, 905.

Dulk, G. A. and Marsh, K. A. 1982, *ApJ*, 259, 350.

Durney, B. R., De Young, D. S., and Roxburgh, I. W. 1993, Sol. Phys., 145, 207.

Fleming, T. A., Giampapa, M. S., Schmitt, J. H. M. M., and Bookbinder, J. A. 1993a, ApJ, 410, 387.

Fleming, T. A., Giampapa, M. S., Schmitt, J. H. M. M., and Bookbinder, J. A. 1993b, ApJ, 410, 387.

Güdel, M. 2002, ARA&A, 40, 217.

Gelino, C. R., Marley, M. S., Holtzman, J. A., Ackerman, A. S., and Lodders, K. 2002, ApJ, 577, 433.

Giampapa, M. S., Rosner, R., Kashyap, V., Fleming, T. A., Schmitt, J. H. M. M., and Bookbinder, J. A. 1996, ApJ, 463, 707.

Gizis, J. E., Monet, D. G., Reid, I. N., Kirkpatrick, J. D., Liebert, J., and Williams, R. J. 2000, AJ, 120, 1085.

Gizis, J. E., Reid, I. N., Knapp, G. R., Liebert, J., Kirkpatrick, J. D., Koerner, D. W., and Burgasser, A. J. 2003, AJ, 125, 3302.

Goldreich, P. and Soter, S. 1966, Icarus, 5, 375.

Gudel, M., Schmitt, J. H. M. M., Bookbinder, J. A., and Fleming, T. A. 1993, ApJ, 415, 236.

Guedel, M. and Benz, A. O. 1993, *ApJ*, 405, L63.

Guedel, M., Benz, A. O., Schmitt, J. H. M. M., and Skinner, S. L. 1996, ApJ, 471, 1002.

Haisch, B., Strong, K. T., and Rodono, M. 1991, Ann. Rev. Astr. Ap., 29, 275.

Hambaryan, V., Staude, A., Schwope, A. D., Scholz, R.-D., Kimeswenger, S., and Neuhäuser, R. 2004, A&A, 415, 265.

Hawley, S. L. *et al.* 2002, AJ, 123, 3409.

Hawley, S. L. *et al.* 1995, ApJ, 453, 464.

Johns-Krull, C. M. and Valenti, J. A. 1996, ApJ, 459, L95+.

Kirkpatrick, J. D. *et al.* 2000, AJ, 120, 447.

Leggett, S. K. *et al.* 2000, ApJ, 536, L35.

Leggett, S. K. *et al.* 2002, ApJ, 564, 452.

Leto, G., Pagano, I., Linsky, J. L., Rodonò, M., and Umana, G. 2000, A&A, 359, 1035.

Liebert, J., Kirkpatrick, J. D., Cruz, K. L., Reid, I. N., Burgasser, A., Tinney, C. G., and Gizis, J. E. 2003, AJ, 125, 343.

Linsky, J. L. and Gary, D. E. 1983, *ApJ*, 274, 776.

Luhman, K. L., Rieke, G. H., Young, E. T., Cotera, A. S., Chen, H., Rieke, M. J., Schneider, G., and Thompson, R. I. 2000, ApJ, 540, 1016.

Martín, E. L. and Ardila, D. R. 2001, AJ, 121, 2758.

Martín, E. L., Basri, G., Delfosse, X., and Forveille, T. 1997, A&A, 327, L29.

Martín, E. L. and Bouy, H. 2002, New Astronomy, 7, 595.

Martín, E. L., Delfosse, X., Basri, G., Goldman, B., Forveille, T., and Zapatero Osorio, M. R. 1999, AJ, 118, 2466.

Mohanty, S. and Basri, G. 2003, ApJ, 583, 451.

Mohanty, S., Basri, G., Shu, F., Allard, F., and Chabrier, G. 2002, ApJ, 571, 469.

Mutel, R. L. and Lestrade, J. F. 1985, AJ, 90, 493.

Neupert, W. M. 1968, ApJ, 153, L59+.

Osten, R., Hawley, S., Allred, J., Johns-Krull, C., and Roark, C. 2004, astro-ph/0411236.

Pizzolato, N., Maggio, A., Micela, G., Sciortino, S., and Ventura, P. 2003, A&A, 397, 147.

Press, W. H., Teukolsky, S. A., Vetterling, W. T., and Flannery, B. P. 1992, Numerical recipes in FORTRAN. The art of scientific computing, (: Cambridge: University Press, |c1992, 2nd ed.).

Putman, M. E. and Burgasser, A. J. 2003, American Astronomical Society Meeting, 203, .

Raedler, K.-H., Wiedemann, E., Meinel, R., Brandenburg, A., and Tuominen, I. 1990, A&A, 239, 413.

Reid, I. N., Gizis, J. E., Kirkpatrick, J. D., and Koerner, D. W. 2001, AJ, 121, 489.

Reid, I. N., Kirkpatrick, J. D., Gizis, J. E., Dahn, C. C., Monet, D. G., Williams, R. J., Liebert, J., and Burgasser, A. J. 2000, AJ, 119, 369.

Reid, I. N., Kirkpatrick, J. D., Gizis, J. E., and Liebert, J. 1999a, ApJ, 527, L105.

Reid, I. N. *et al.* 1999b, ApJ, 521, 613.

Roberts, D. H., Lehar, J., and Dreher, J. W. 1987, AJ, 93, 968.

Rosner, R., Golub, L., and Vaiana, G. S. 1985, ARA&A, 23, 413.

Rutledge, R. E., Basri, G., Martín, E. L., and Bildsten, L. 2000, *ApJ*, 538, L141.

Saar, S. H. and Linsky, J. L. 1985, *ApJ*, 299, L47.

Schweitzer, A., Gizis, J. E., Hauschildt, P. H., Allard, F., and Reid, I. N. 2001, ApJ, 555, 368.

Shkolnik, E., Walker, G. A. H., and Bohlender, D. A. 2003, ApJ, 597, 1092.

Smith, E. J., Davis, L., Jones, D. E., Coleman, P. J., Colburn, D. S., Dyal, P., and Sonett, C. P. 1975, Science, 188, 451.

Soderblom, D. R., Stauffer, J. R., Hudon, J. D., and Jones, B. F. 1993, ApJS, 85, 315.

Stelzer, B. 2004, ApJ, 615, L153.

Stepanov, A. V., Kliem, B., Zaitsev, V. V., Fürst, E., Jessner, A., Krüger, A., Hildebrandt, J., and Schmitt, J. H. M. M. 2001, A&A, 374, 1072.

Stevenson, D. J. 1991, ARA&A, 29, 163.

Vrba, F. J. *et al.* 2004, AJ, 127, 2948.

West, A. A. *et al.* 2004, AJ, 128, 426.

Zapolsky, H. S. and Salpeter, E. E. 1969, ApJ, 158, 809.

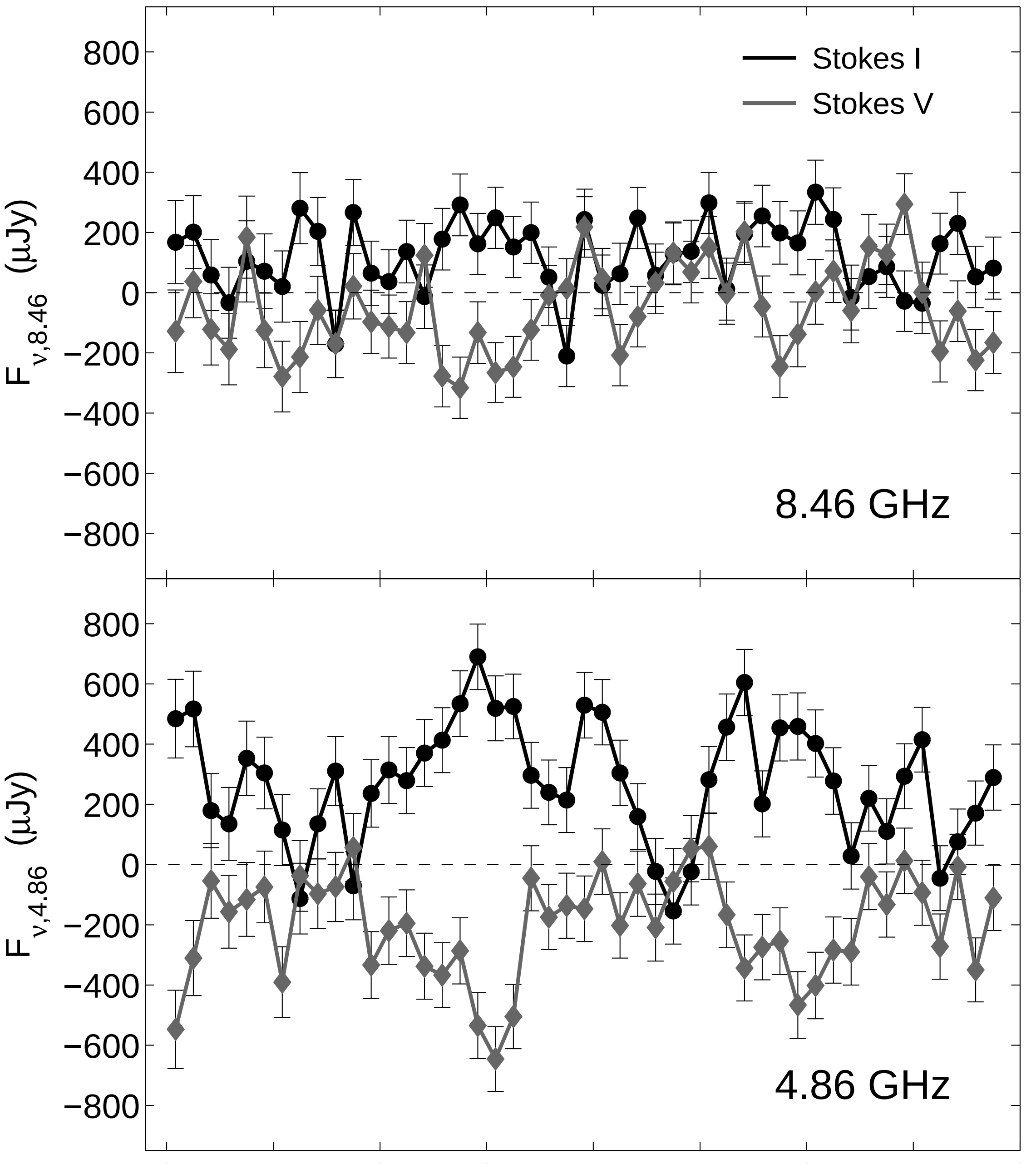

FIG. 1.— Radio light curves of 2MASS J00361617+1821104 at 8.5 GHz (top) and 4.9 GHz (bottom). Both total intensity (black circles) and circular polarization (gray diamonds) are shown, with a 10-min time resolution. The negative sign of the circularly-polarized flux indicates left-handed polarization. The light curves for both frequencies and polarizations are variable, though with lower significance at 8.5 GHz (§6).

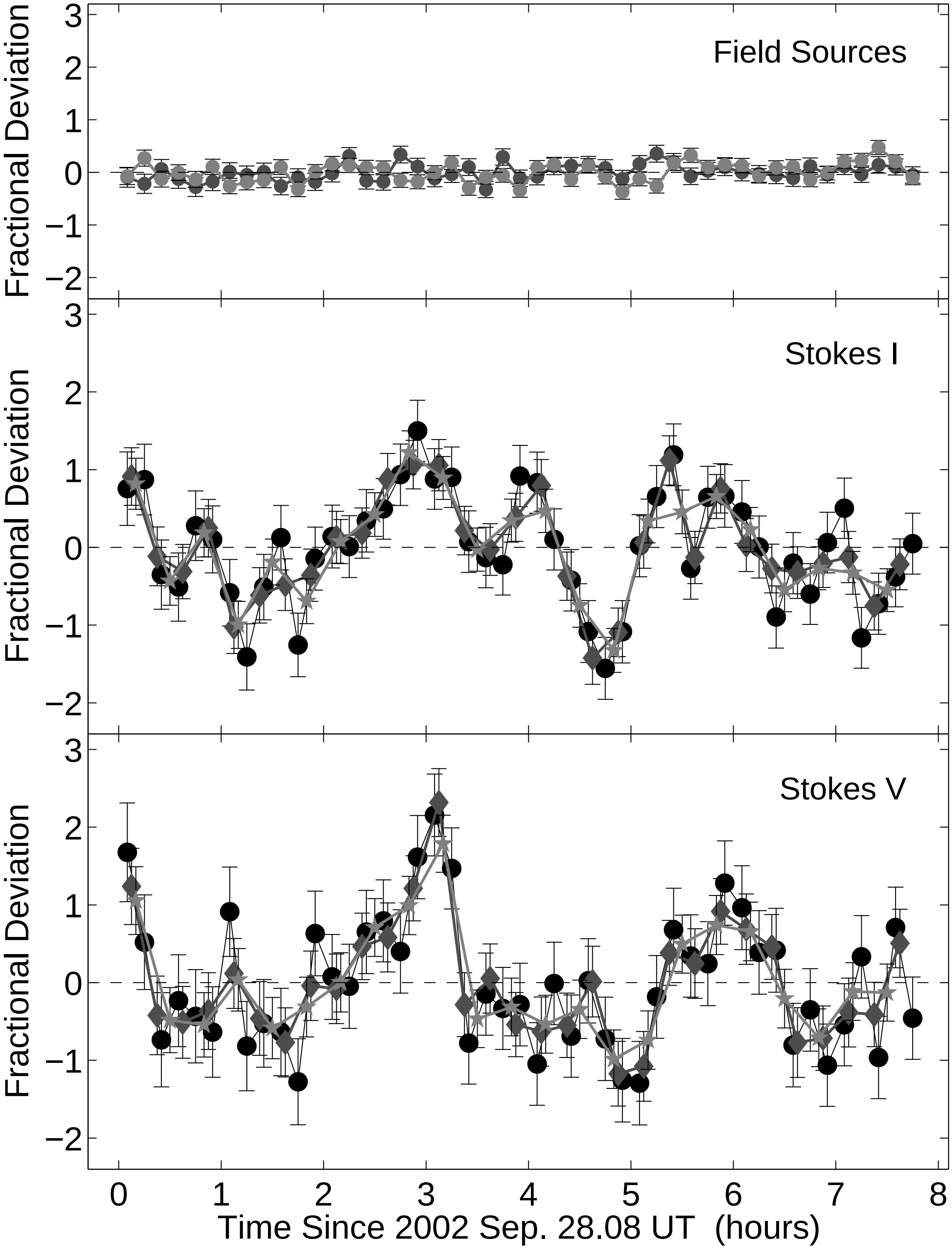

FIG. 2.— Fractional deviation relative to the mean of the circular polarization (bottom) and total intensity (middle) light curves of 2MASS J00361617+1821104 at 4.9 GHz. Time resolutions of 10, 15, and 20 minutes are plotted. The top panel shows the light curves of two field sources with a 10-min time resolution. Clearly, the emission from 2M0036+18 is highly variable independent of time resolution. The light curve of 2M0036+18 also appears to be periodic with a period of about 3 hours.

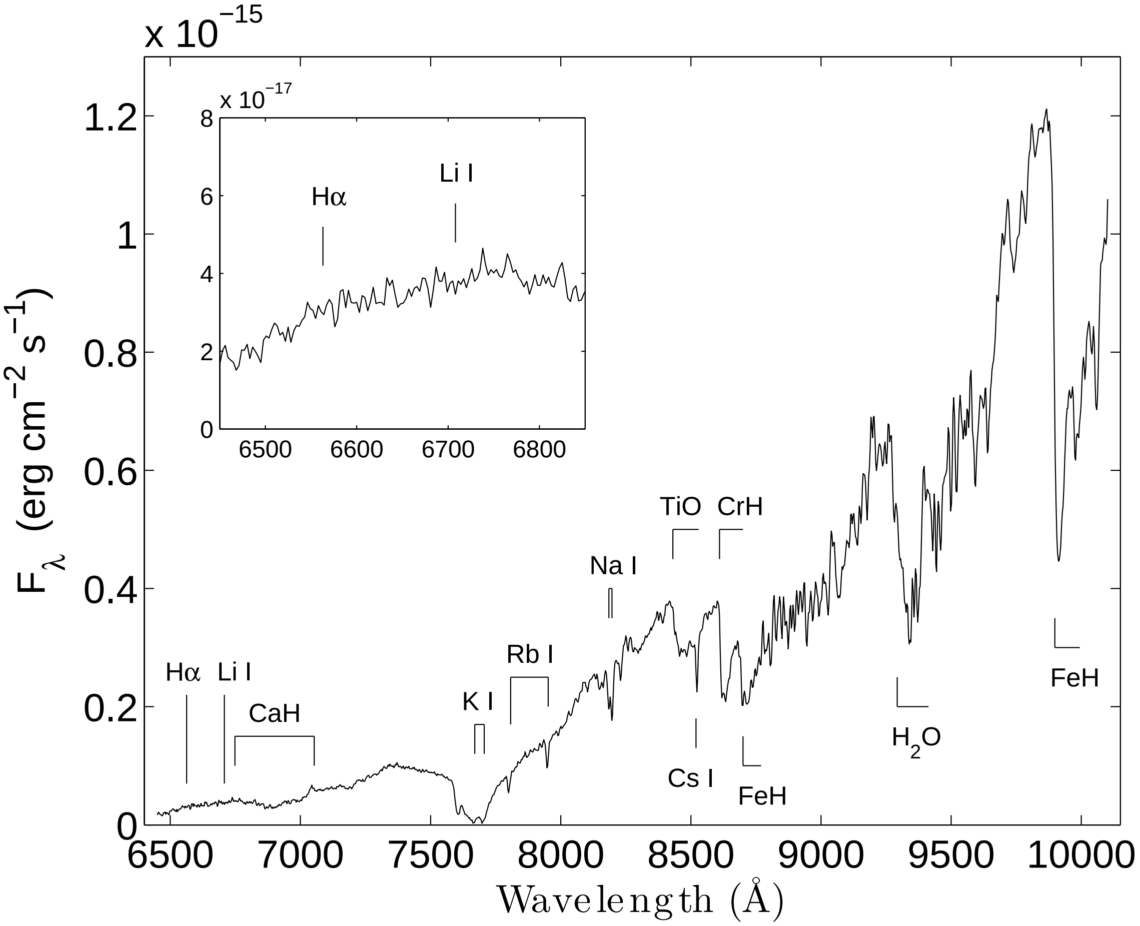

FIG. 3.— Combined 4-hour optical spectrum of 2M0036+18. The location of Hα and prominent absorption features are marked. Clearly, no Hα emission is detected above the continuum level (inset).

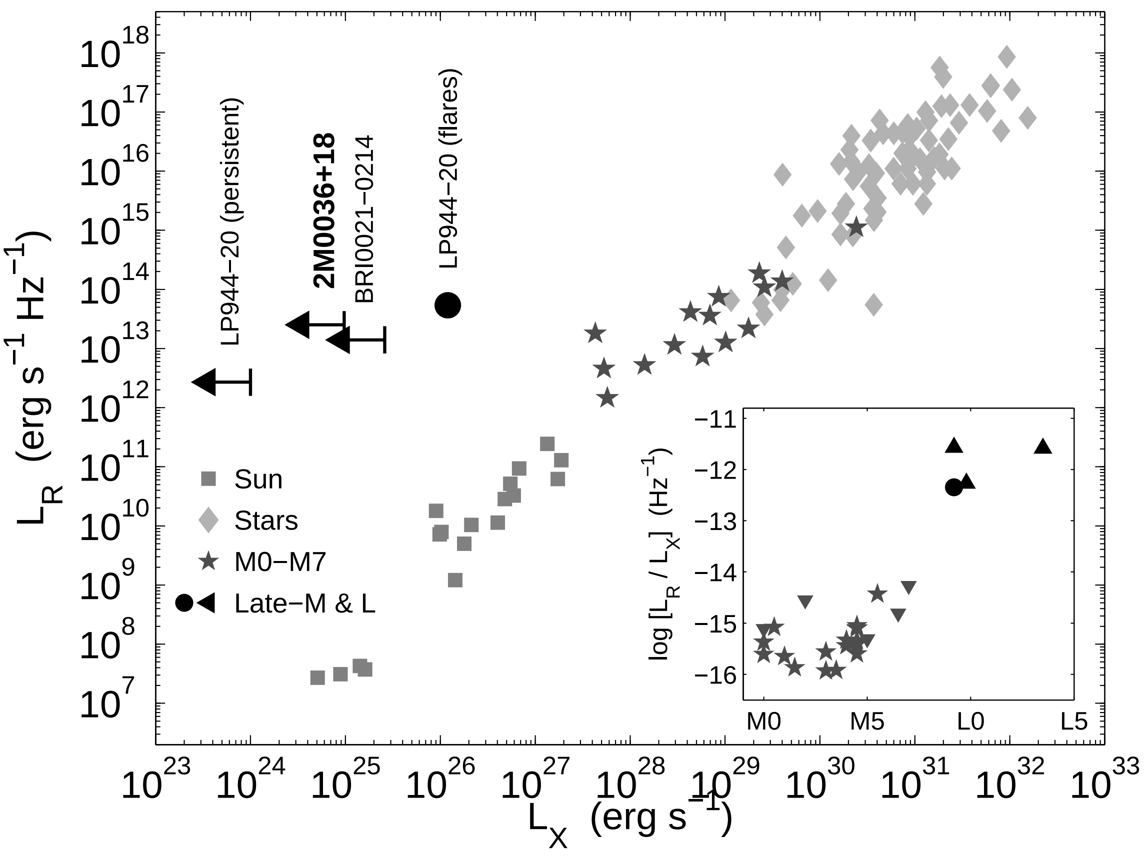

FIG. 4.— Radio versus X-ray luminosity for stars exhibiting coronal activity. Data for late-M and L dwarfs are from B01 and B02, while other data are taken from Güdel (2002) and references therein. Data points for the Sun include impulsive and gradual flares, as well as microflares. The strong correlation between L_R and L_X is evident and extends to spectral type M7 (see inset). Clearly, 2MASS J00361617+1821104 and the other late-M and L dwarfs detected in the radio to date violate the correlation by many orders of magnitude.

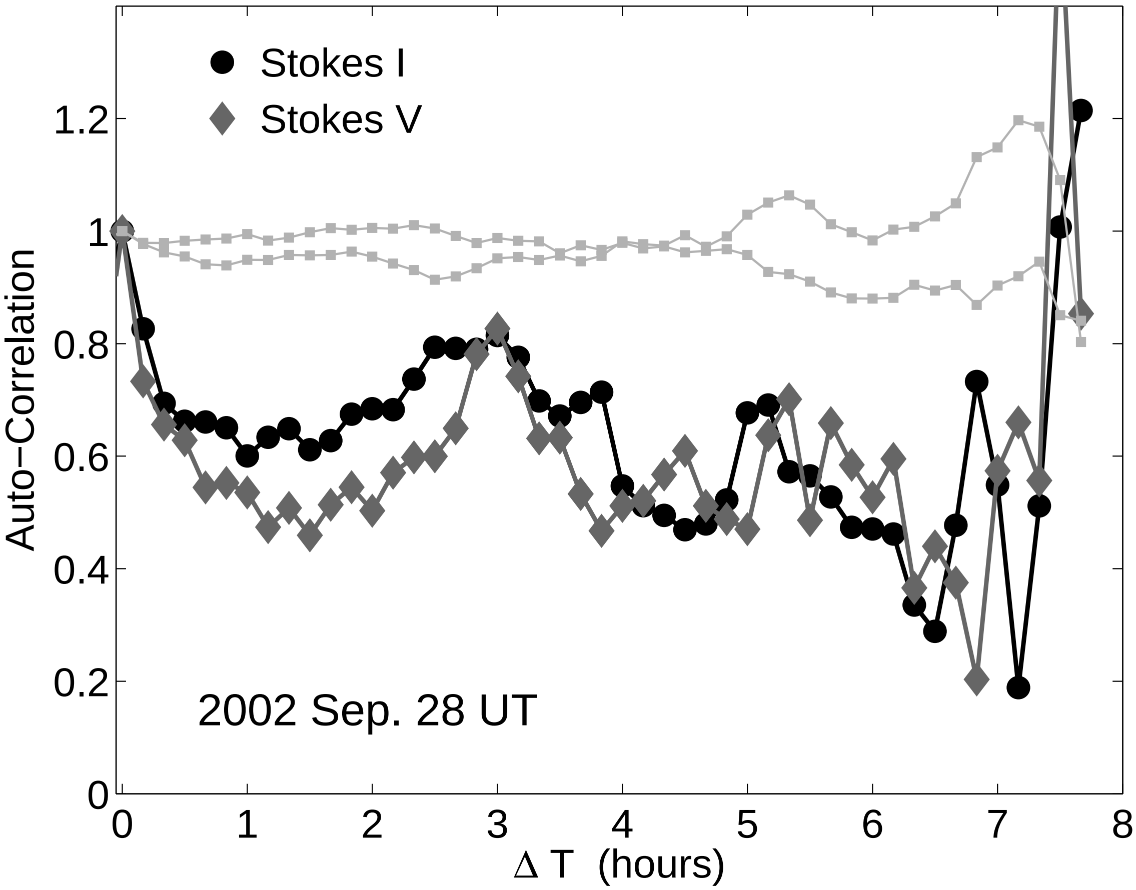

FIG. 5.— Auto-correlation function (ACF) as a function of temporal lag for the total intensity (black circles) and circular polarization (gray diamond) light curves of 2MASS J00361617+1821104, as well as two field sources (gray squares). The time resolution is 10 minutes (thick lines and field sources). A clear peak in the ACF of 2M0036+18 is seen at a lag of 3 hours. The flat ACF of the field sources is indicative of a non-periodic signal. The timescale of about 1 hour on which the signal from 2M0036+18 de-correlates (i.e., the first minimum in the ACF) indicates that the covering fraction of the emission region is $\sim$ 10%.

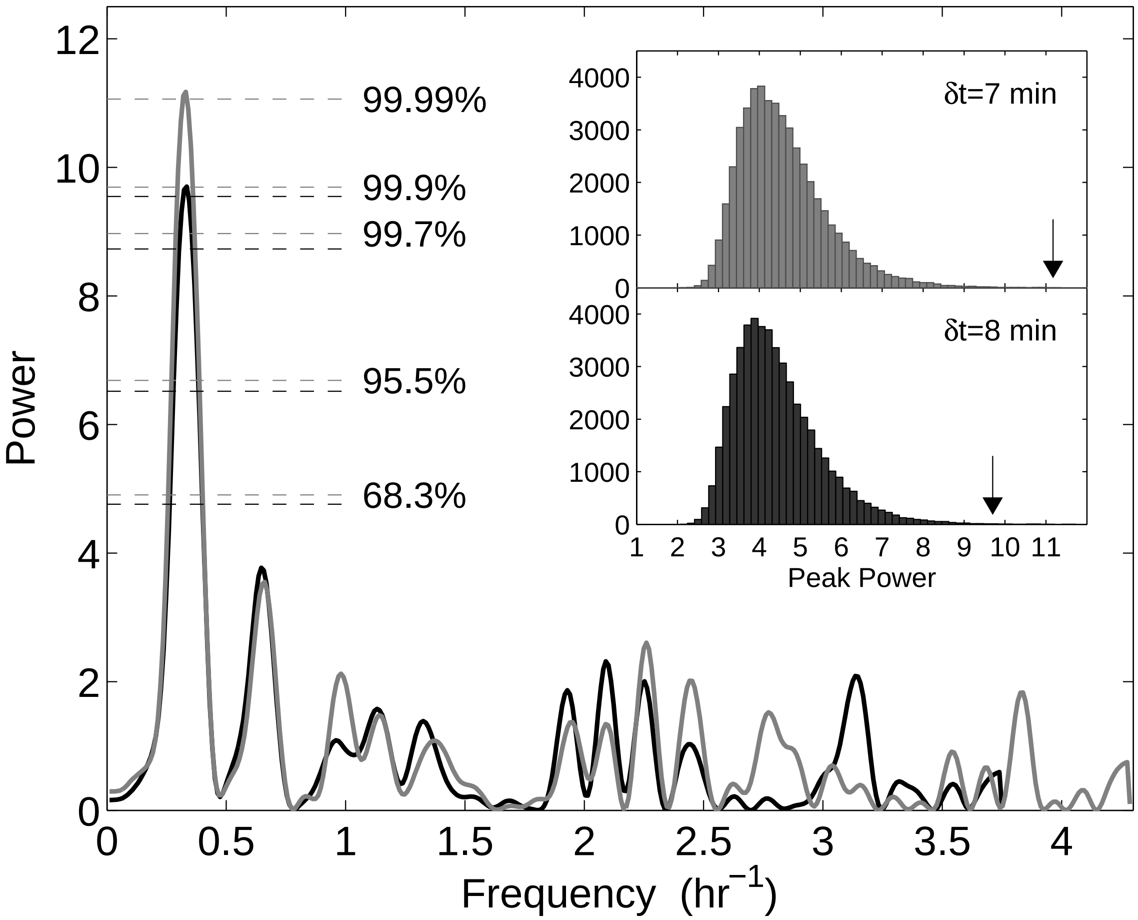

FIG. 6.— Lomb-Scargle periodogram for the circularly polarized emission at 4.9 GHz with a time resolution of 8 min (black) and 7 min (gray). The dashed lines indicate the 68.3%, 95.5%, 99.7%, 99.9%, and 99.99% significance levels based on Monte Carlo simulations of 50,000 randomized versions of the light curve (inset). For both time resolutions the most significant peak (99.9% and 99.99%) is at a frequency of 0.33 hr^{-1}, or a period of 3.0 hours. We find the same result, though with different significance (see Figure 7), for both total intensity and circular polarization at a wide range of time resolutions.

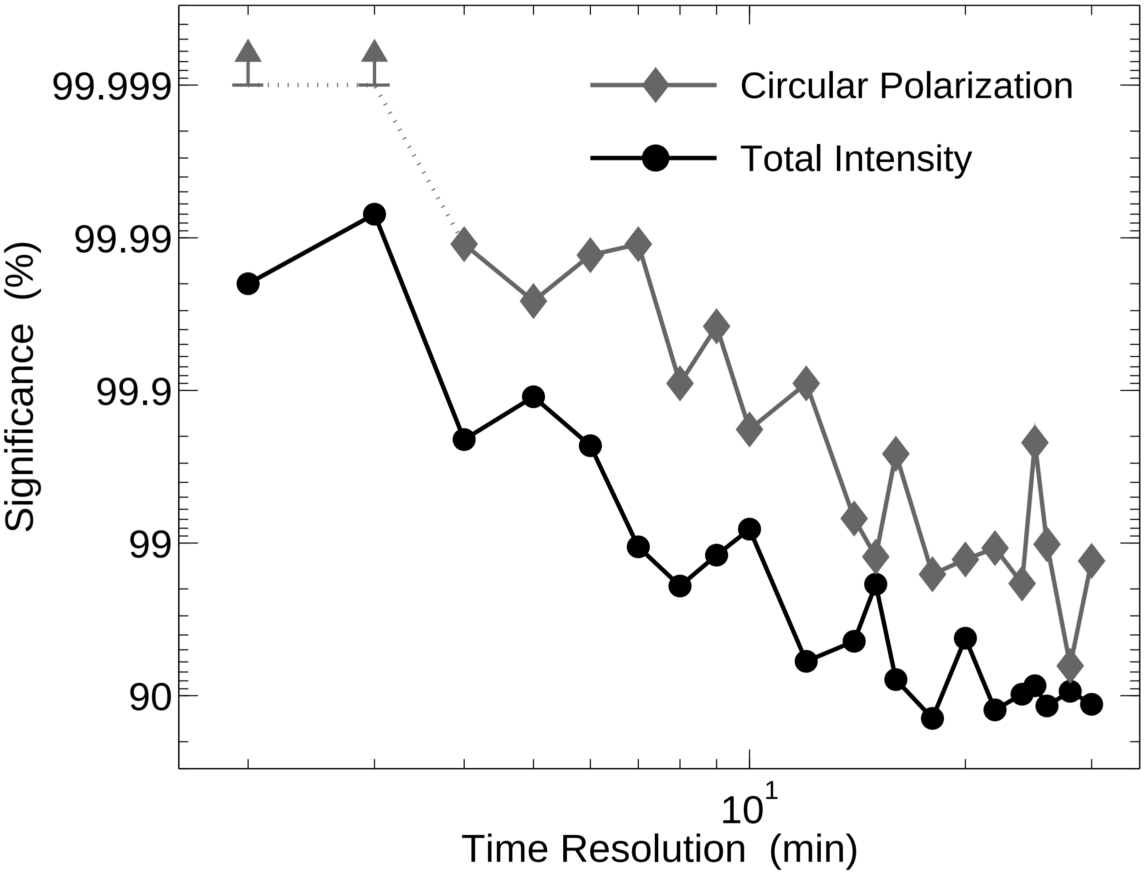

FIG. 7.— Significance of the 3-hour period in the total intensity (black) and circular polarization (gray) 4.9 GHz light curves as a function of time resolution. The significance is determined using Monte Carlo simulated and randomized light curves as described in §6 and shown in Figure 6.

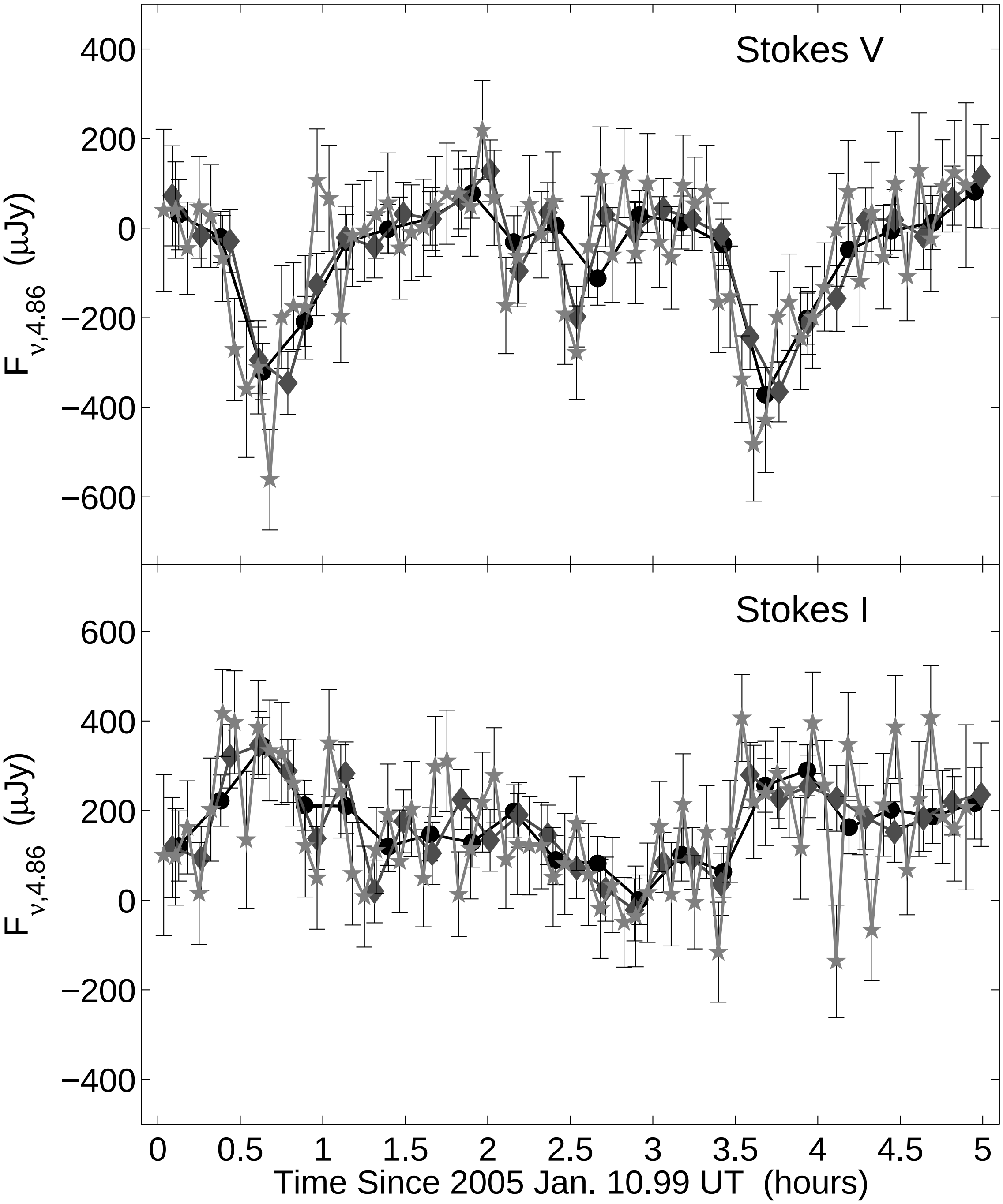

FIG. 8.— Follow-up observations of 2M0036+18 at 4.86 GHz taken on 2005, Jan. 10.99 UT for a total of 5 hours. The 3-hour period detected in the initial observations from Sep. 2002 is clearly seen.

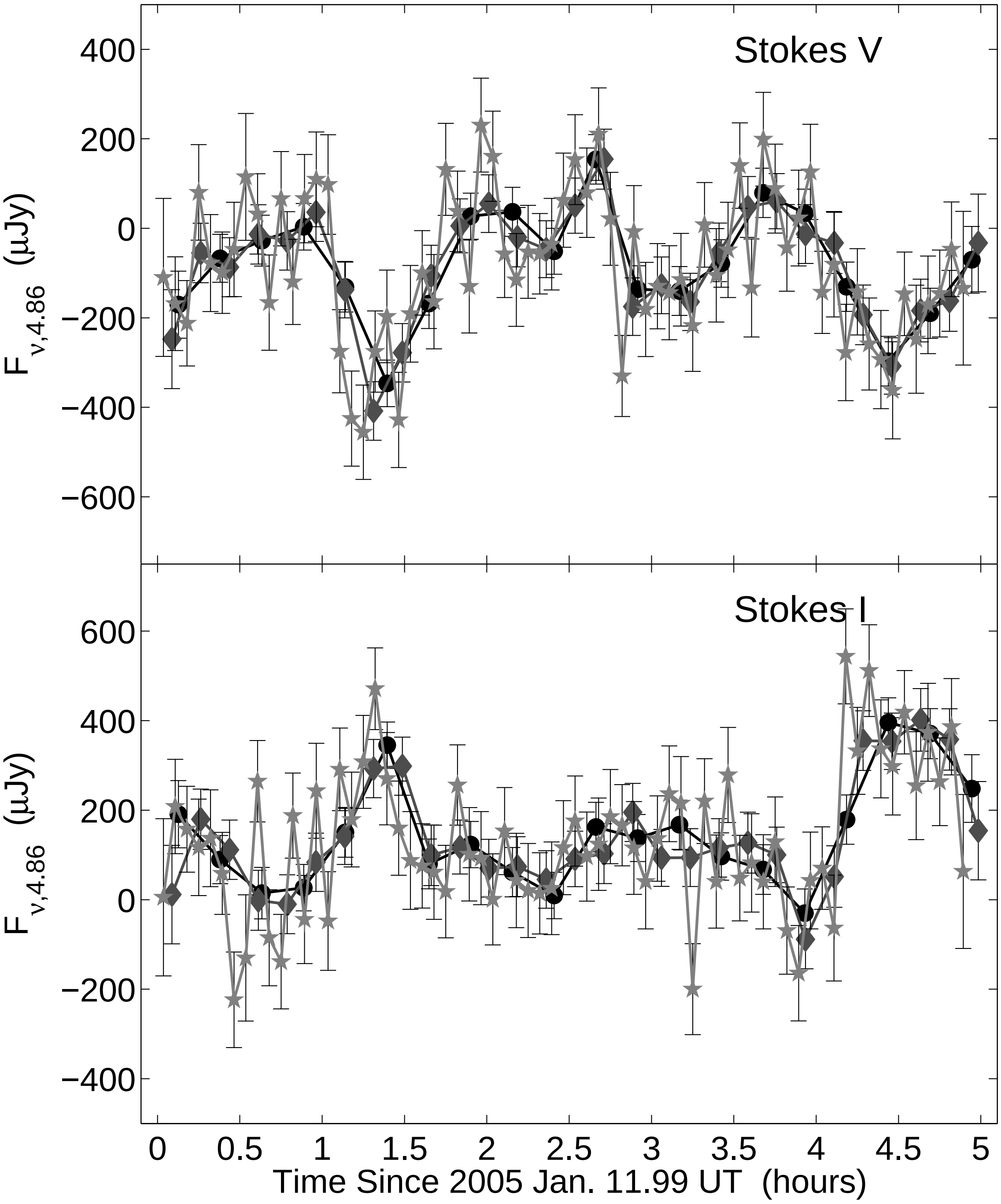

FIG. 9.— Follow-up observations of 2M0036+18 at 4.86 GHz taken on 2005, Jan. 11.99 UT for a total of 5 hours. The 3-hour period detected in the initial observations from Sep. 2002 is clearly seen.

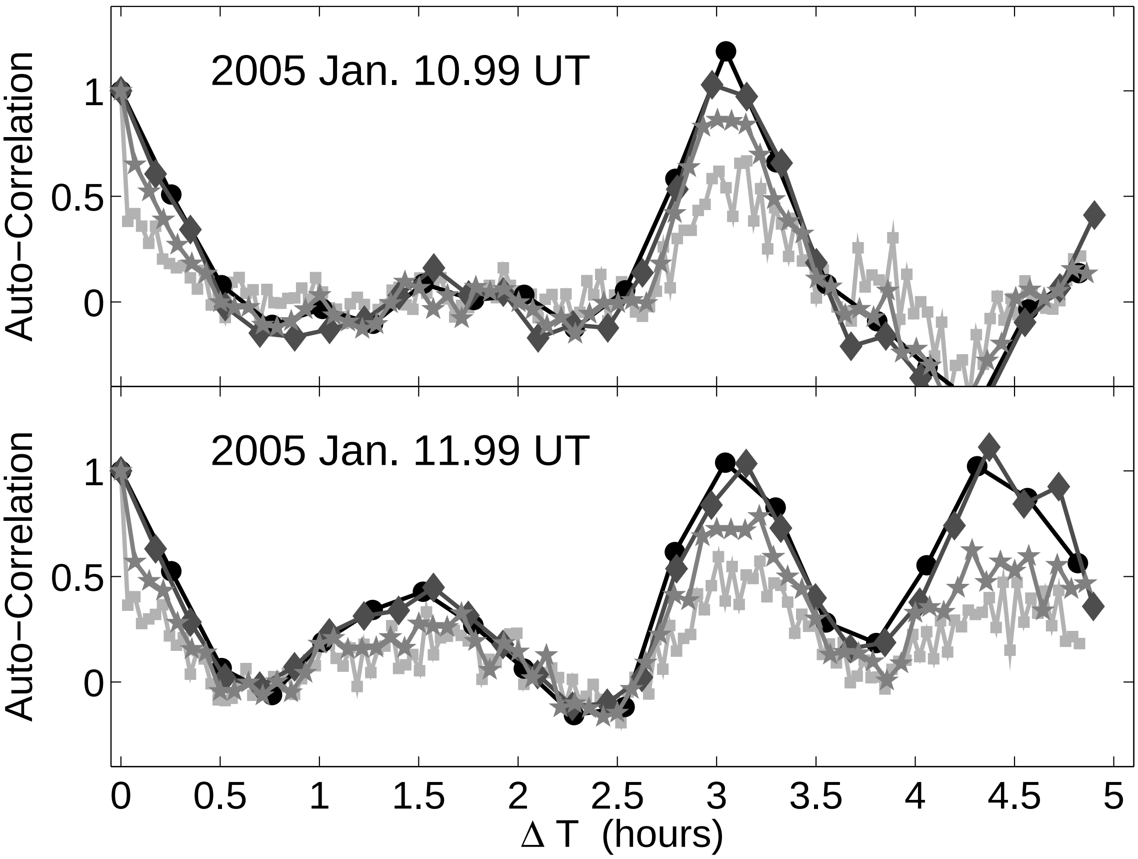

FIG. 10.— Auto-correlation function (ACF) as a function of temporal lag for circular polarization in the follow-up observations on Jan. 10 (top) and Jan. 11 (bottom). The time resolution ranges from 2 to 15 min. A clear peak is seen at a lag of 3 hours, with a fall-off time of about 1 hour, confirming the periodicity.

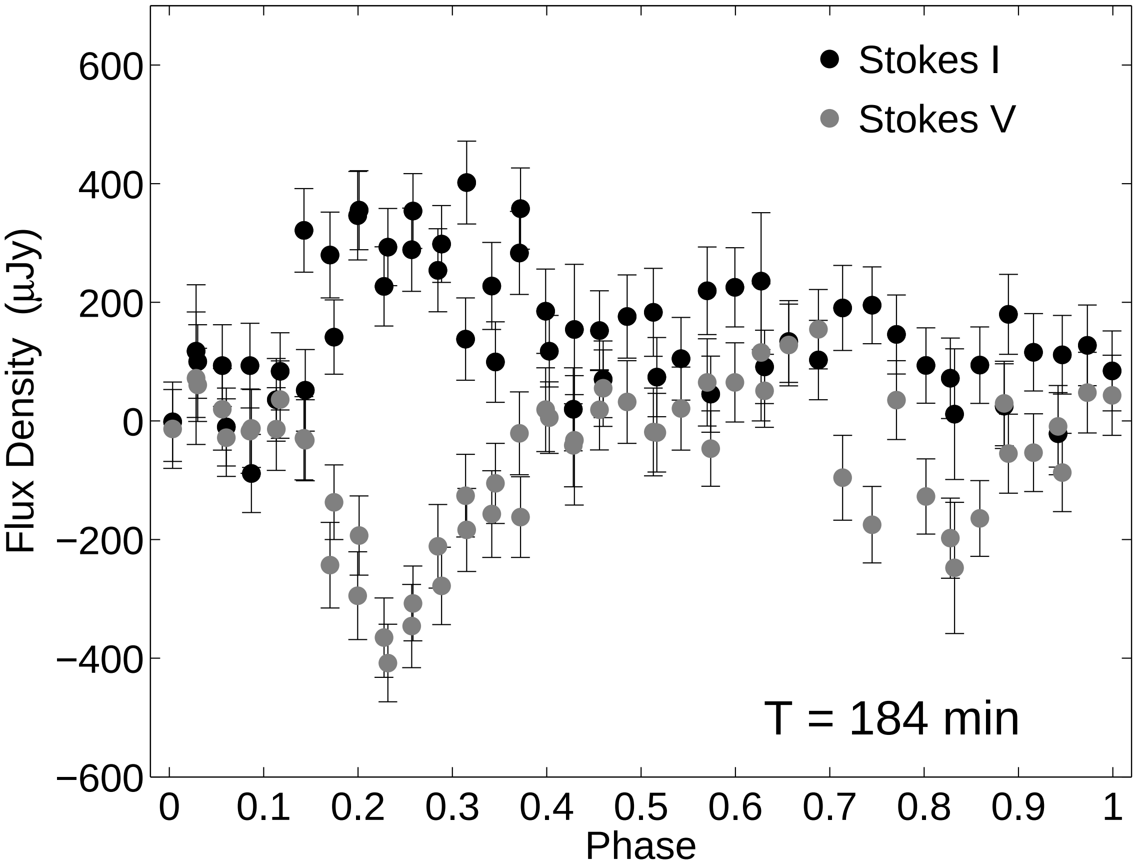

FIG. 11.— Phased light curve (total intensity and circular polarization) for the observations from Jan. 10 and 11 UT folded with a period of 184 min.

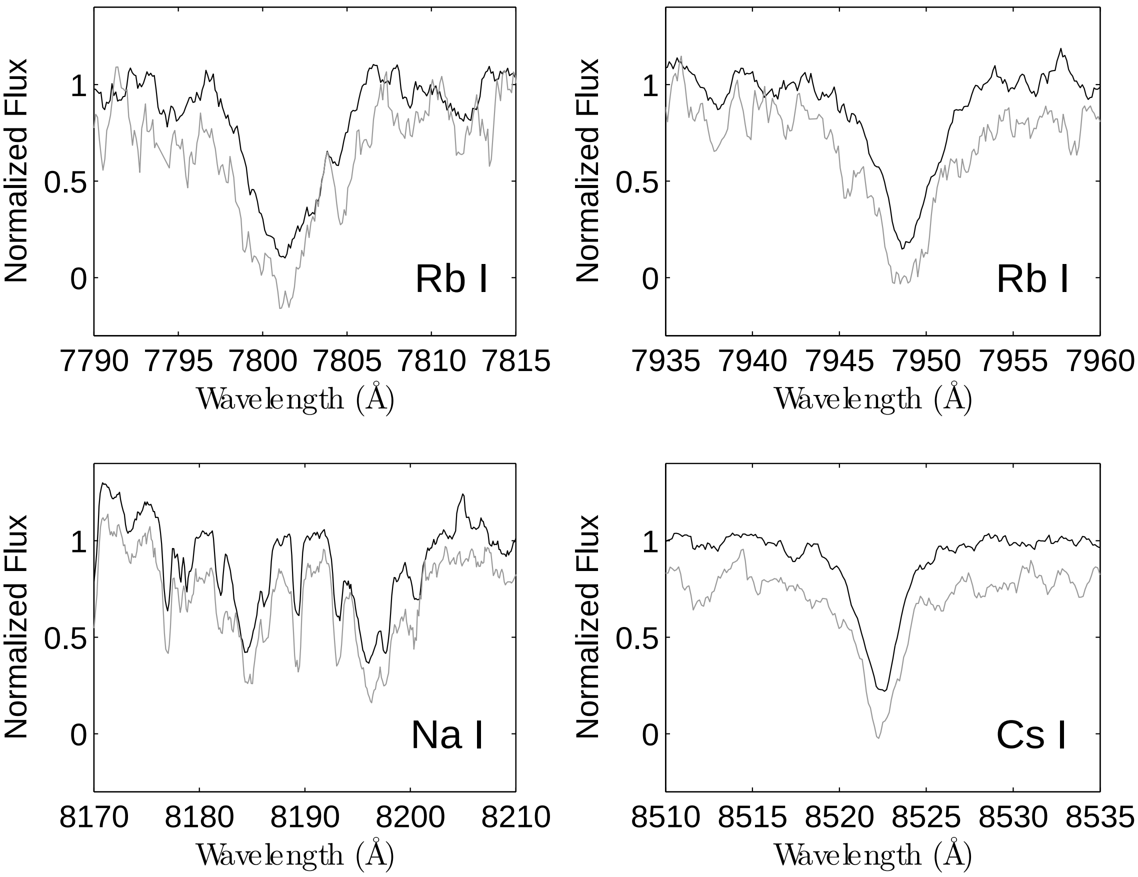

FIG. 12.— Zoom-in on four spectral features in the high-resolution MIKE spectra of 2M0036+18, smoothed by two times the instrumental resolution. The second spectrum has been offset downward for clarity. No obvious shift in the lines is discernible.

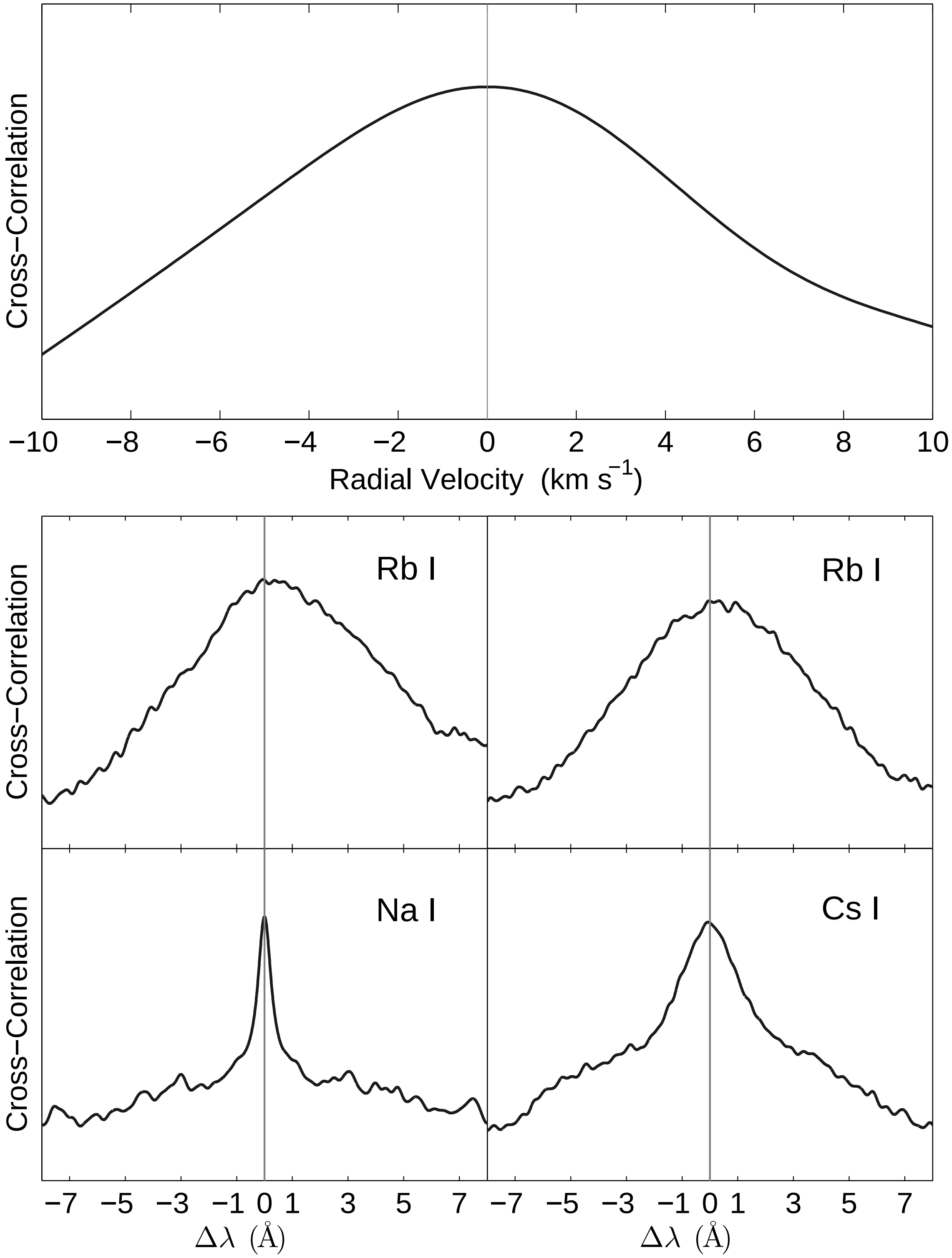

FIG. 13.— Cross-correlation of the two MIKE spectra using the orders in which strong absorption lines were detected. The peak is at zero shift indicating no detectable radial velocity signature between the two epochs. The limiting factor in the accuracy of this result is the width of the absorption features.

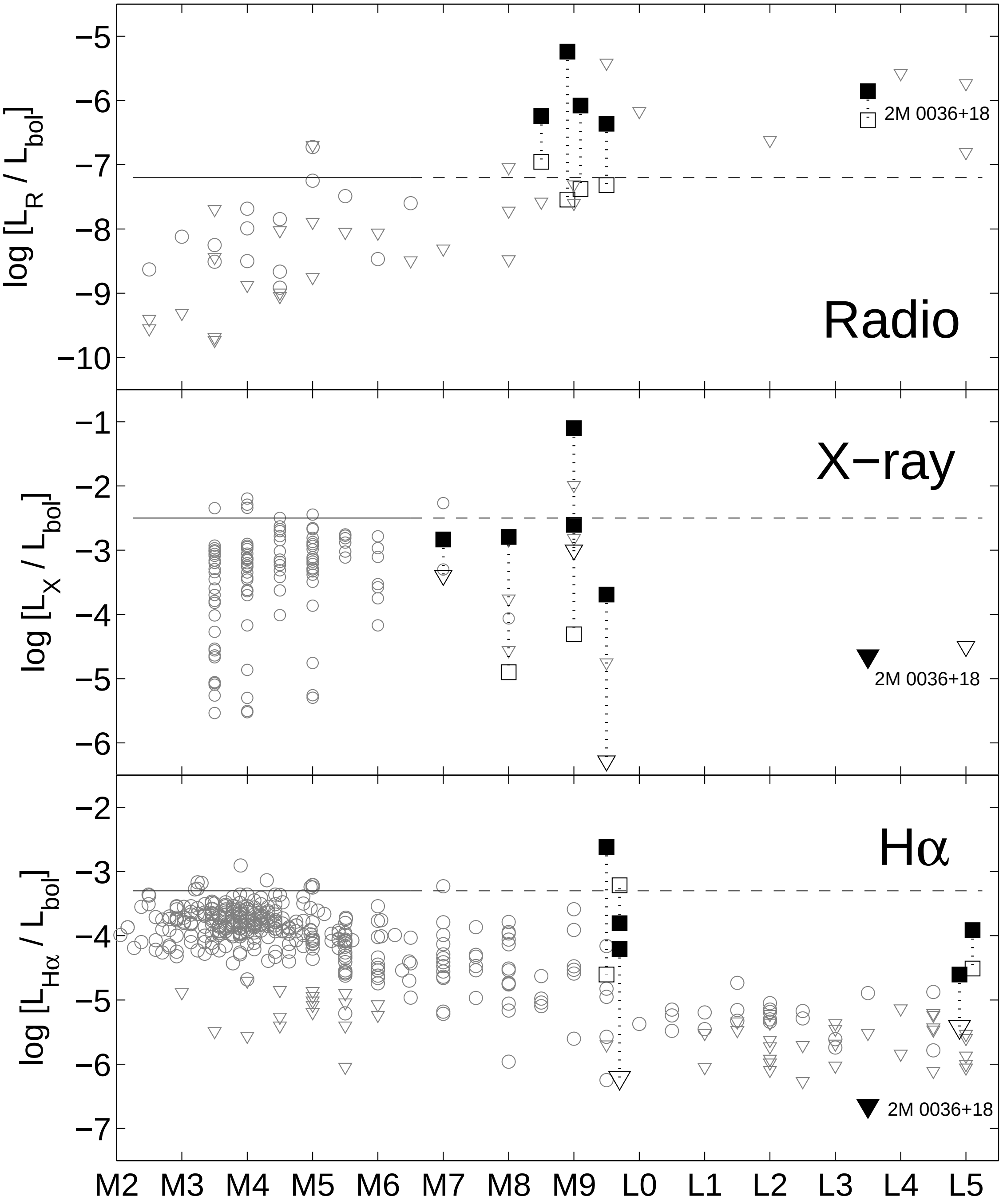

FIG. 14.— Radio (top), X-ray (middle) and Hα (bottom) activity as a function of spectral type. Shown are objects with flares (solid squares) and persistent emission (detections: open squares; upper limits: triangles), as well as objects with persistent emission only (detections: circles; upper limits: triangles). The solid line in each panel marks the maximum level of activity for spectral types earlier than M7, and the dashed lines are an extrapolation to later spectral types. In both X-rays and Hα the level of persistent activity drops significantly beyond M7, while flares occasionally reach the same level of activity of early M dwarfs. In the radio band, on the other hand, several objects exhibit activity levels much stronger than that observed in early M dwarfs. This is particularly pronounced in the case of 2M0036+18.

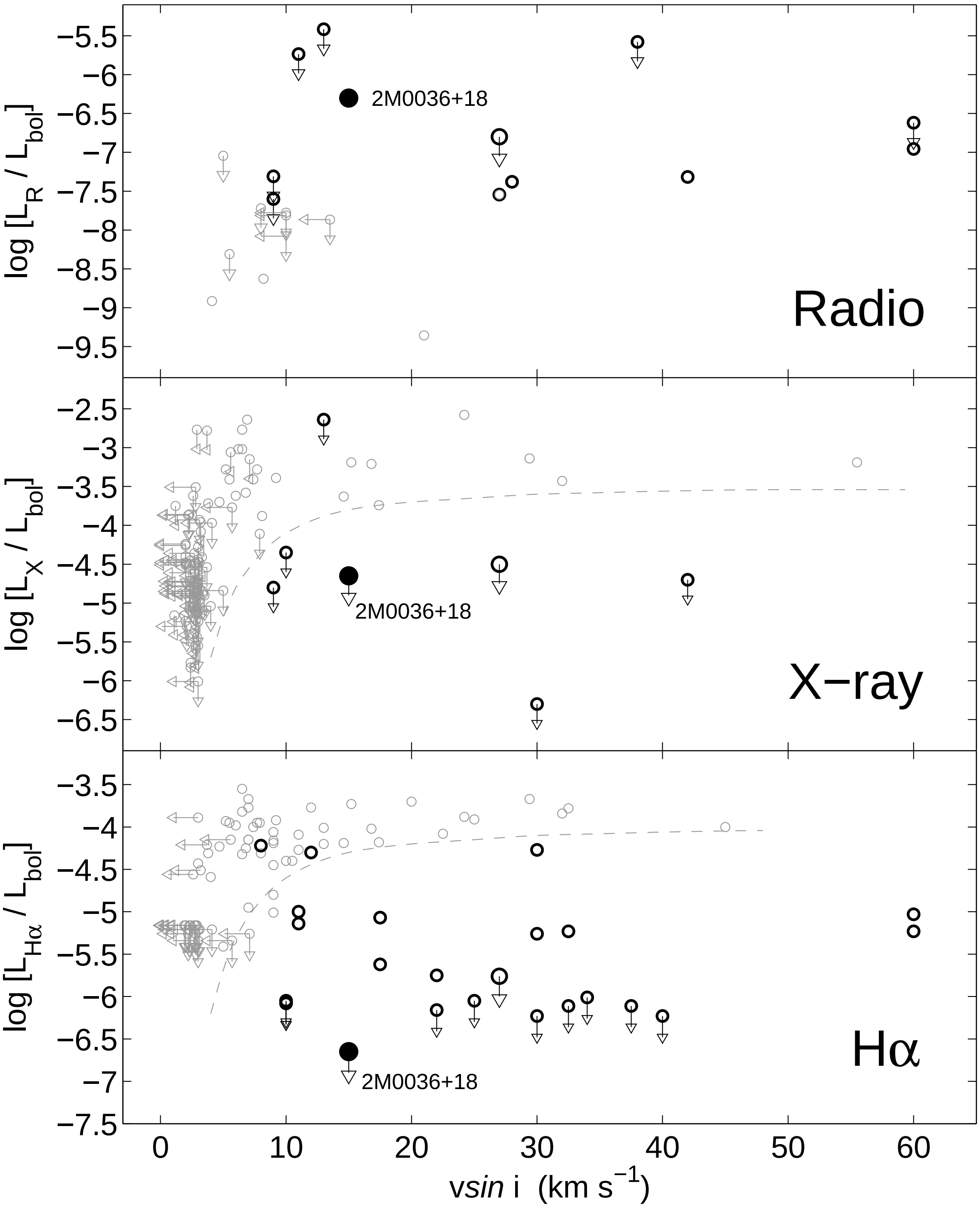

FIG. 15.— Radio (top), X-ray (middle) and Hα (bottom) activity as a function of rotation velocity. M dwarfs up to spectral type M8 are shown in gray symbols, while dwarfs later than M8 are shown in black symbols. The early M dwarfs exhibit a clear rotation-activity relation in Hα and X-rays (gray dashed lines). This relation breaks down in the late-M and L dwarfs with many fast rotators exhibiting no Hα or X-ray emission. In the radio, on the other hand, faster rotation appears to be correlated with activity even for dwarfs later than M9. The large open circle designates the L5 dwarf 2M 1507-16 (see Appendix).